Exploratory Analysis of Wave Problems on Thin and Singular Structures[1]

William Graham[2]

September 13, 2018

[1]SAMBa MRes Project, University of Bath MA50248
[2]Supervisor: Dr. Kirill Cherednichenko, University of Bath

Contents

Chapter 1

Background and Preliminaries

1.1 Optical- and Photonic Crystal- Fibres

Optical fibres are the *de facto* industry standard for large telecommunications systems, thanks to their ability to transmit information quickly and with far less signal loss than other methods (such as metal cables). The technology has rapidly developed since the first optical fibres were fabricated in the 1970s [1] and optical fibres in use today present a balance between several competing factors to deliver a reliable performance. Factors such as (optical) loss are inherent, brought about by the materials needed to build the fibres; whilst other factors can be influenced by design (group-velocity dispersion) or the fabrication process (which can lead to imperfections and polarisation effects). Despite the technological developments of the fibres, the underpinning physical processes remain unchanged — all improvements to the technology have been incremental and largely centre around the manufacturing process. The fibre will have a core made of a dielectric (non-conducting) material with a given refractive index, N_{core} and will be surrounded by cladding, another dielectric material of a different index N_{cladding} (Figure 1.1(a)). The fibre then relies on total internal refraction (TIR) to guide light along the fibre. When a light ray in the core strikes the core-cladding boundary Snell's law determines the angle at which the light ray propagates upon entering the cladding[1],

$$N_{\text{core}} \sin\theta_{\text{i}} = N_{\text{cladding}} \sin\theta_{\text{t}}; \tag{1.1}$$

where θ_{i} and θ_{t} are (respectively) the angles of incidence and transmission from the boundary. It's possible for $\theta_{\text{t}} > \frac{\pi}{2}$ provided that $N_{\text{core}} > N_{\text{cladding}}$; in which case (TIR happens and) the light ray does not enter the cladding at a refracted angle, but rather is totally reflected and continues propagating through the core. Equation (1.1) can also be used to show that the component of the wavevector parallel to the core-cladding interface, $k_p = N_{\text{core}} k \sin(\theta_{\text{i}})$, remains unchanged during the interaction and so is constant along the fibre for a given mode[2]. For any given material with refractive index N, all values $k_p \leq Nk$ allow light to propagate in the medium[3], and for each k_p the modal index is defined as $N_{\text{m}} = \frac{k_p}{k}$. To form a guided mode light must have a value of k_p which cannot propagate in the cladding but which can propagate in the core, which can be satisfied by ensuring that

$$\begin{aligned} N_{\text{cladding}} k \leq k_p \leq N_{\text{core}} k \\ \Leftrightarrow N_{\text{cladding}} \leq N_{\text{m}} \leq N_{\text{core}}. \end{aligned}$$

[1] The "deflection" of the ray as it passes between the materials is the well-known phenomenon of refraction.
[2] A mode is a single solution to the wave equation in the fibre.
[3] This is an upper bound as it's derived by looking at an infinite, homogeneous "slab" of the material.

Photonic crystals can be used as cladding for a conventional fibre; these crystals also have a maximal value of k_p which allows light to propagate in them, and this maximal value defines an "effective refractive index" in accordance with $N_{\text{eff}} = \frac{k_p}{k}$. Therefore, if at a particular frequency (equivalently k, however it is conventional to work with the frequency here) $N_{\text{eff}} < N_{\text{core}}$, the photonic crystal can be used as cladding material and will guide light via a form of TIR. Photonic crystal *fibres* (PCFs) are a departure from the setup of core surrounded by cladding [2]; instead relying on the microstructure of the photonic crystal to alter the optical properties of the fibre it forms. This microstructure can cause the crystal to exhibit band-gaps; frequency ranges[4] where there are no propagating modes of light in the crystal, despite the existence of propagating modes at lower (and/or higher) frequencies. The important revelation comes in the fact that band-gaps can appear for frequencies corresponding to $N_{\text{eff}} < 1$, which means that light in vacuum at these frequencies will be confined if surrounded by such a crystal - making "hollow-core" fibres possible. The term hollow-core refers to a PCF with vacuum as its "core material", PCFs can also be "solid-core" with another material in them (Figure 1.1(b)). Crucially though, these fibres do not use TIR to guide light but rather exploit the fact that light at particular frequencies is confined simply because it is unable to propagate in the surrounding crystal, due to the optical properties bestowed on the crystal by its microstructure. Figure 1.1 illustrates the difference in fibre design between optical fibres and PCFs.

PCFs have been the subject of a number of mathematical models in recent years. The standard starting point for these models is the time-harmonic system of Maxwell equations

$$\nabla \wedge \mathbf{E} = i\omega\mu\mathbf{H}, \qquad \nabla \wedge \mathbf{H} = -i\omega\varepsilon_{\text{p}}, \mathbf{E}$$

where $\mathbf{E}$ and $\mathbf{H}$ are the electric and magnetic (-displacement) fields respectively, and the medium in

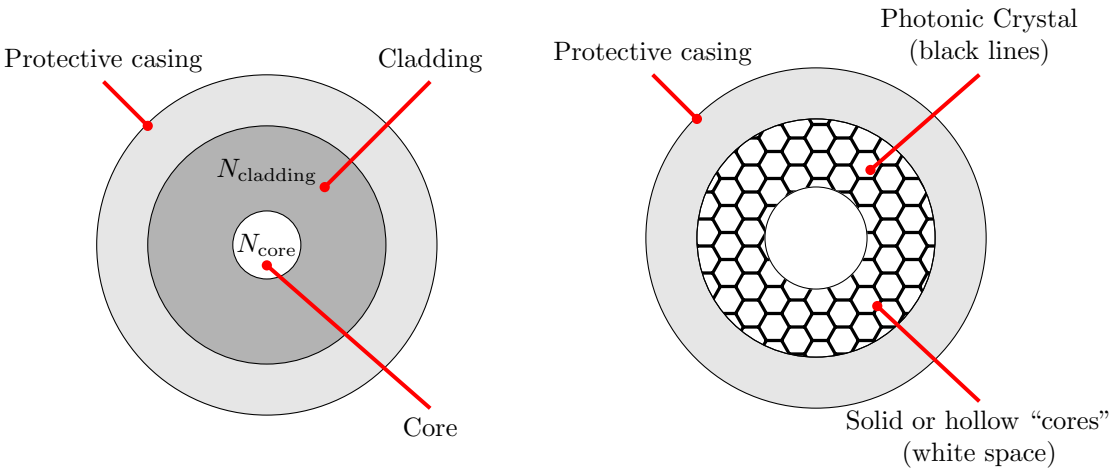

(a) Cross-sectional design of an optical fibre, which uses TIR to guide light. Modes are restricted to the core by the choice of k_p and as $N_{\text{core}} > N_{\text{cladding}}$.

(b) Cross-section of a PCF which uses the existence of photonic band gaps to confine light. The photonic crystal is represented by the black hexagons whilst the solid/hollow cores are the white fillings.

Figure 1.1: Difference in the cross-sectional structure of an optical fibre and a PCF. The optical fibre will guide modes within a given modal (index) range. The PCF microstructure vary, and certain structures can be engineered to confine different frequencies of light.

[4]Respectively k-ranges or N_m ranges, [1], [2].

which the problem is posed has electric permittivity ε_{p}[5] and magnetic permeability μ. Note that the reason for using the time-harmonic Maxwell system arises from consideration of the fibre structure[6] and seeking solutions via a wave ansatz of the form $\hat{\mathbf{E}} = \mathbf{E}e^{i(k_p z - \omega t)}$ (and similarly for the magnetic field); these are referred to as Bloch waves. Further assumptions are also made on the fields, namely that the amplitude coefficients $\mathbf{E}, \mathbf{H}$ are functions of x, y only, and do not vary along the fibre. This assumption is well-grounded as these models are seeking waves that will propagate down the fibre, and expect the $\mathbf{E}$ and $\mathbf{H}$ fields to vary only in the plane perpendicular to the direction of propagation. As for the domain of the problem which describes the microstructure and hence the fibre, models assume a unit cell (commonly taken to be the unit square) and periodically extend the domain from this. The unit cell itself is taken to be composed of two materials with different material constants, which means ε_{p} and μ become piecewise-constant functions of the (x, y) variables. This provides a general model for any kind of periodic structure, rather than the specific geometry we will restrict ourselves to in future. Analysis of this model and the solution properties can be found in (for example) [3] and [4]. The approach is to apply homogenisation theory due to the periodic structure of the domain, and introduce an appropriate representation of a periodic problem on the unit cell. One can then prove convergence results for various aspects of the unit-cell problem and the original periodic problem (most notably the spectrum of the problem, which determines the frequencies ω of light which can propagate). The work in [4] makes a few more assumptions on the model and produces results relating to the decay of certain solutions as well. When the task is to find solutions to the Maxwell system, one often turns to numerical schemes to produce approximations for visualisation. The use of the time-harmonic Maxwell equations means that methods such as the Finite Element Method can be used, and there is no need to incorporate time-variation into the numerical scheme, which is a bonus in terms of computation time and algorithm complexity.

In summary, PCFs present a "cautiously optimistic" improvement to the current industry standard. The physical theory underlying the process by which they operate means that PCFs have the potential to replace optical fibres as the industry standard. This is not a simple case of fabricating better fibres, but rather there are several industry standards that will need to be met before PCFs are accepted and implimented over optical fibres [1]. However PCFs have an advantage over optical fibres in that their applications are not only limited to telecommunications. At present prominant aternative applications include (but are not limited to) nonlinear optics (where they offer high optical intensities per unit power, making them highly efficient) and atom and particle guidance (dielectric particles can be guided by the dipole forces exerted by light). Hence there has been much to motivate study of the optical properties of PCFs, and understand how the design (geometry of the fibre, fabrication material) affects these, resulting in the models based on the Maxwell equations and development of spectral convergence results for periodic problems.

1.2 Singular Structure Problems

We will be looking to analyse problems posed on singular structures (to motivate the discussion in Chapter 4) and so present some theory that will justify the methods we use. We restrict ourselves to cases that are directly applicable to the analysis we are looking to perform, and so focus on graphs embedded in Euclidean space $\mathbb{R}^d$, and which exhibit periodic structure in each dimension. The theory extends beyond this [5], being applicable in much more general settings and with graphs that have other complicating factors. These more general problems are sometimes referred to as "quantum

[5]The subscript being used to distinguish the microstructure length scale ε (which will be introduced later) and electric permittivity in the event of confusion.

[6]That is, as a 2-dimensional periodic structure extended into three dimensions as a prism.

graphs".

Let $\mathbb{G} = (V, E)$ be a graph with set of vertices V and edges E. Suppose further that $\mathbb{G}$ is embedded in $\mathbb{R}^d$; namely that each $v_i \in V$ can be associated with a point $\mathbf{v}_i \in \mathbb{R}^d$ and each $e_{ij} = (v_i, v_j) \in E$ can be identified with the line segment joining $\mathbf{v}_i$ and $\mathbf{v}_j$. With this identification of vertices and edges we can use subsets of $\mathbb{R}^d$ to describe subgraphs of $\mathbb{G}$, and vice-versa. If $U \subset \mathbb{R}^d$ (for example), then the "part of $\mathbb{G}$ in U" is the subgraph which consists of all vertices whose associated point lies in U, and all edges between those points whose associated line segment lies entirely in U. Concepts such as translations and rotations of the graph can also be understood as being applied to the associated points and segments in $\mathbb{R}^d$. We also impose some periodic structure on $\mathbb{G}$; which is to say that there exists some finite subset $\mathcal{U} \subset \mathbb{R}^d$ and corresponding subgraph $\mathbb{G}_\mathcal{U}$ such that $\mathbb{G}$ is a (possibly infinite) union of translations of $\mathbb{G}_\mathcal{U}$. Colloquially, $\mathbb{G}$ can be assembled by stacking (in each of the d-dimensions) copies of the graph $\mathbb{G}_\mathcal{U}$. We use the term "*unit cell* of $\mathbb{G}$" to refer to this subset $\mathcal{U}$ or subgraph $\mathbb{G}_\mathcal{U}$. Without loss of generality we take the unit cell of $\mathbb{G}$ to be a (hyper-) cube of side length l.

We denote the space of complex-valued square-integrable functions on $\mathbb{G}$ by $L^2(\mathbb{G})$. Identifying each edge e_{ij} with some one-dimensional interval $I_{ij} \subset \mathbb{R}$, any $u \in L^2(\mathbb{G})$ can be identified with a set of "edge"-functions $\{u_{ij} : I_{ij} \to \mathbb{C}\}$. Next, we let $\mathcal{A}$ be an operator defined on functions $u \in L^2(\mathbb{G})$; of the form $\mathcal{A}u = -\nabla \cdot (A\nabla u)$, and whose spectrum we wish to obtain. This requires solving the eigenvalue-eigenfunction equation

$$-\nabla \cdot (A\nabla u) = \omega^2 u$$

for $\omega \in \mathbb{R}$ and[7] $u \in L^2(\mathbb{G})$. Solutions are found by solving

$$-\frac{\mathrm{d}}{\mathrm{d}x}\left(a_{ij}\frac{\mathrm{d}}{\mathrm{d}x}u\right) = \omega^2 u$$

on each of the intervals I_{ij} (also described as solving "on the edges e_{ij}"), and appropriate matching conditions at the vertices, to give $u \in L^2(\mathbb{G})$ in terms of it's edge components. Here a_{ij} is just the appropriate restriction of A to the edge e_{ij}. For periodic graphs it is customary to apply a Gelfand transform to $\mathcal{A}$ to aid in analysis of these problems, which provides a way of representing the operator $\mathcal{A}$ in terms of a family of operators $\mathcal{A}^\Theta$. Here $\Theta = (\theta_1, \theta_2, ..., \theta_d)$ is a parameter of the family of operators $\mathcal{A}^\Theta$ that we need to study, and the θ_i are the quasi-momenta (one for each periodic direction of the graph) which range over[8] $[-\frac{\pi}{l}, \frac{\pi}{l})$. The Gelfand transform then represents $\mathcal{A}$ as a direct integral of the operators $\mathcal{A}^\Theta$ over the quasi-momenta[9]. Importantly, the Gelfand transform means that determining the spectrum of $\mathcal{A}$ can be done by determining the spectrum of $\mathcal{A}^\Theta$ and taking the union over all $\theta_1, \theta_2, ..., \theta_d$. It is this fact which we shall make use of in the analysis of the following problems.

It should be noted that several assumptions and simplifications have been made in the above discussion, the details of which will not be elaborated on. The foremost of these is the construction of the Hilbert space $L^2(\mathbb{G})$, and the fact that the Gelfand transform has to be extended by L^2-closure to be applicable to (operators on) non-smooth functions. Furthermore, when applying the Gelfand transform to graphs embedded in $\mathbb{R}^d$ we have assumed the graph is periodic in all d-directions, however

[7] The operator $\mathcal{A}$ is self-adjoint, and hence has a real spectrum. The choice of ω^2 (presupposing an entirely real spectrum) is posthumously justified in later sections.

[8] The quasi-momenta have a range determined by the size of the period cell in each dimension. As we assume a (hyper-) cube period cell, each quasi-momentum has the same range. For more general unit cells, different quasi-momentum will have different ranges.

[9] The Gelfand transform can be seen as a generalisation of the familiar Fourier transform. Indeed, the Fourier transform *is* the Gelfand transform in a specific context.

in general the graph may be periodic in $d' < d$ directions. For a graph periodic in one direction and with a finite periodic cell, an auxiliary procedure called "flattening" can be applied to the graph before the Gelfand transform, to reduce the complexity of the setup. An example of (and a description of the flattening proceedure) a graph embedded in $\mathbb{R}^d$ but only periodic in only one dimension can be found in [6].

1.3 Discussion of Length and Frequency Scalings

Besides singular structure problems we will also consider problems posed on thin-structure periodic domains in $\mathbb{R}^d$. Denote such a domain by Ω; which similarly to the periodic graphs is composed of translations of a unit cell, but which (unlike the singular-structure problems) possess microstructure on a different length scale to the unit cell. We assume (without loss of generality) that the period cell is a (hyper-) cube with side length 1, with microstructure of length scale ε, denoted by P_ε. In this section we aim to briefly introduce the various frequency frameworks that exist for problems of this kind, and how they are interlinked. Analogously to Section 1.2 we are interested in the spectrum of the operator $\mathcal{A}u = -\nabla \cdot (A\nabla u)$ for $u \in L^2(\Omega)$ and so examine the eigenvalue-eigenfunction equation

$$-\nabla \cdot (A\nabla u) = \omega^2 u. \tag{1.2}$$

The expressions $P_\varepsilon + \mathbf{x}$ for $\mathbf{x} \in \mathbb{R}^3$ are interpreted as the translation of all points in the unit cell P_ε by the vector $\mathbf{x}$, and αP_ε as the scaling of the unit cell P_ε by the scalar α. To setup the finite-frequency approximation we introduce the domain length scale N, which for simplicity we shall take to be a multiple of the side-length of our periodic unit cell (so $N \in \mathbb{N}$). Next we construct another (related) problem on a finite domain Ω_F; which we construct by stacking N^d copies of P_ε, with N stacked along each axis so that

$$\Omega_F = \bigcup_{x,y,z \in \{0,1,\ldots,N\}} \left(P_\varepsilon + (x,y,z)^\top\right) \subset [0,N]^3.$$

At the boundary of Ω_F we impose periodic boundary conditions; these effectively mimic the fact that Ω fills the whole of $\mathbb{R}^d$ with some periodic structure, and our finite-frequency approximation is looking for solutions which are periodic across N unit cells. with periodic boundary conditions imposed on $\partial\Omega_F$. We still seek solutions to (1.2) on Ω_F, only now $u \in L^2(\Omega_F)$. Hence in the finite-frequency approximation we are looking to find the spectrum of the operator $\mathcal{A}_N$, defined on functions $u \in L^2(\Omega_F)$. Passing to the limit $N \to \infty$ results in the spectrum of the operators $\mathcal{A}_N$ converging to the spectrum of the operator in the full space ($\mathcal{A}$).

Having established a finite-frequency approximation it makes sense to talk about alternative frequency approximations. One can think of a high-frequency approximation to the original problem; which is posed on a (hyper-) cubic domain of side length 1, but composed of N^d copies of $\frac{1}{N}P_\varepsilon$ (stacked). This domain,

$$\Omega_H = \frac{1}{N}\Omega_F = \bigcup_{x,y,z \in \{0,\frac{1}{N},\ldots,1\}} \left(\frac{1}{N}P_\varepsilon + (x,y,z)^\top\right) \subset [0,1]^3,$$

again has periodic boundary conditions on $\partial\Omega_H$, and again we obtain a sequence of operators (parametrised by N) and their corresponding spectra. In the limit $N \to \infty$ this gives us the spectrum of an operator on a finite, homogenised domain. Additionally we can move between the high- and finite-frequency

approximations using a domain-length-scale (and complimentary frequency-scale) change: in the high-frequency regime we have the problem

$$-\nabla \cdot (A(\mathbf{x}) \nabla u(\mathbf{x})) = \omega^2 u(\mathbf{x}), \quad \mathbf{x} \in \Omega_H, \tag{1.3}$$

and rescaling the domain-length-scale via $\mathbf{y} = N\mathbf{x}$, (1.3) becomes

$$-\frac{1}{N}\nabla_{\mathbf{y}} \cdot \left(A(\mathbf{y}) \frac{1}{N} \nabla_{\mathbf{y}} u(\mathbf{y}) \right) = \omega^2 u(\mathbf{y}), \qquad \mathbf{y} \in \Omega_F \tag{1.4}$$

$$\Leftrightarrow -\nabla_{\mathbf{y}} \cdot (A(\mathbf{y}) \nabla_{\mathbf{y}} u(\mathbf{y})) = (N\omega)^2 u(\mathbf{y}), \qquad \mathbf{y} \in \Omega_F, \tag{1.5}$$

which implies that the accompanying frequency scaling $\omega \to N\omega$ can be used to understand the spectrum in one frequency approximation, given the spectrum of the other. The relationship between the original system and the high- and finite-frequency regimes is illustrated in Figure 1.2, for a two-dimensional problem.

A note on convention at this point - throughout this report we will refer to ω as "eigenfrequencies", and ω^2 as the eigenvalues. This is because a large portion of our analysis will focus on determining ω, rather than ω^2 and so provide a clear naming convention to make this distinction. However we will often refer to the spectrum of some operator in terms of the eigenfrequencies ω, rather than the eigenvalues ω^2 — when this is done we refer to the spectrum composed of the eigenvalues ω^2 which correspond to the eigenfrequencies ω. Lastly we remark that the choice of finite-frequency or baseline approximation determines the language used to describe the other frequency approximation, as these are all relative. We could have chosen (perfectly reasonably) to call the problem in Ω_H the finite-frequency approximation, in which case the problem in Ω_F would be called a low-frequency approximation. In this report we shall be working in the former case, that is with Ω_F labelled the finite-frequency problem.

1.4 Asymptotic Regimes, Thin Structure Problems and Band Gap Spectra

Having chosen a frequency approximation to work with (and adopting the setup from the previous section), the two length scales N, ε now present us with various asymptotic limits to explore, which can be used to inform us about the spectrum of the original problem. The end goal of analysing the "effective problem" is to provide a means of estimating[10] the spectrum of the original problem by way of understanding a simpler problem, or alternatively to obtain a problem in which an analytic approach is feasible. Let us denote the periodic full-space domain with microstructure-length scale ε as Ω_ε; the case $\varepsilon = 0$ is regarded as the singular-structure domain and so has associated embedded graph $\mathbb{G}$. Introducing the domain-length scale N gives us set of finite-frequency domains $\Omega_{\varepsilon,N}$ on which we want to find the spectrum, $(\sigma_{\varepsilon,N})$, of the appropriate operator $\mathcal{A}_{\varepsilon,N}$ on $u \in L^2(\Omega_{\varepsilon,N})$. We denote this eigenvalue problem by $\mathcal{P}_{\varepsilon,N}$. Each of the limits $N \to \infty$ and $\varepsilon \to 0$ then provides us with a sequence of problems $(\mathcal{P}_{\varepsilon,N})$ and an associated sequence of spectra $(\sigma_{\varepsilon,N})$ which converges to the spectrum of an operator that acts on functions in the full-space. Taking $\varepsilon = \varepsilon^* > 0$ as fixed for example, and sending $N \to \infty$ provides a sequence of problems whose spectra $\sigma_{\varepsilon^*,N} \to (0, \infty)$ as $N \to \infty$, which is the spectrum of a periodic thin-structure medium occupying the whole of $\mathbb{R}^d$. One

[10] Formally it is necessary to qualify this notion of estimate and associated convergence, as we are considering a limit of a sequence of sets and so the meaning of convergence is not obvious. One may interpret this convergence in the Hausdorff sense, for example.

can obtain approximations to each $\sigma_{\varepsilon^*,N}$ numerically, using e.g. the finite element method which we do in Chapter 3).

Other limits involving $\varepsilon \to 0$ offer more variety in the resulting effective problems. In these limits the microstructure becomes singular structure, and the periodic cell can be represented by a graph (hence these problems are referred to as singular structure problems). The edges and vertices of this graph are determined by the geometry of the unit cell; but colloquially the edges represent the "zero-thickness" microstructure, and the vertices "junctions" or connections - this is illustrated in Figure 1.3. The effective problem is a singular-structure problem and so the theory discussed in Section 1.2 is applicable. The domain is a periodic graph $\mathbb{G} = (V, E)$ on which we are seeking the spectrum of the operator $\mathcal{A}_{0,N}$. The appropriate boundary conditions to apply at the vertices depend on the scaling of the so-called edge-"volume" $V^{(\mathrm{E})}$ and vertex-"volume"[11] $V^{(\mathrm{V})}$ [7] in Ω. The relative scaling of $V^{(\mathrm{V})}$

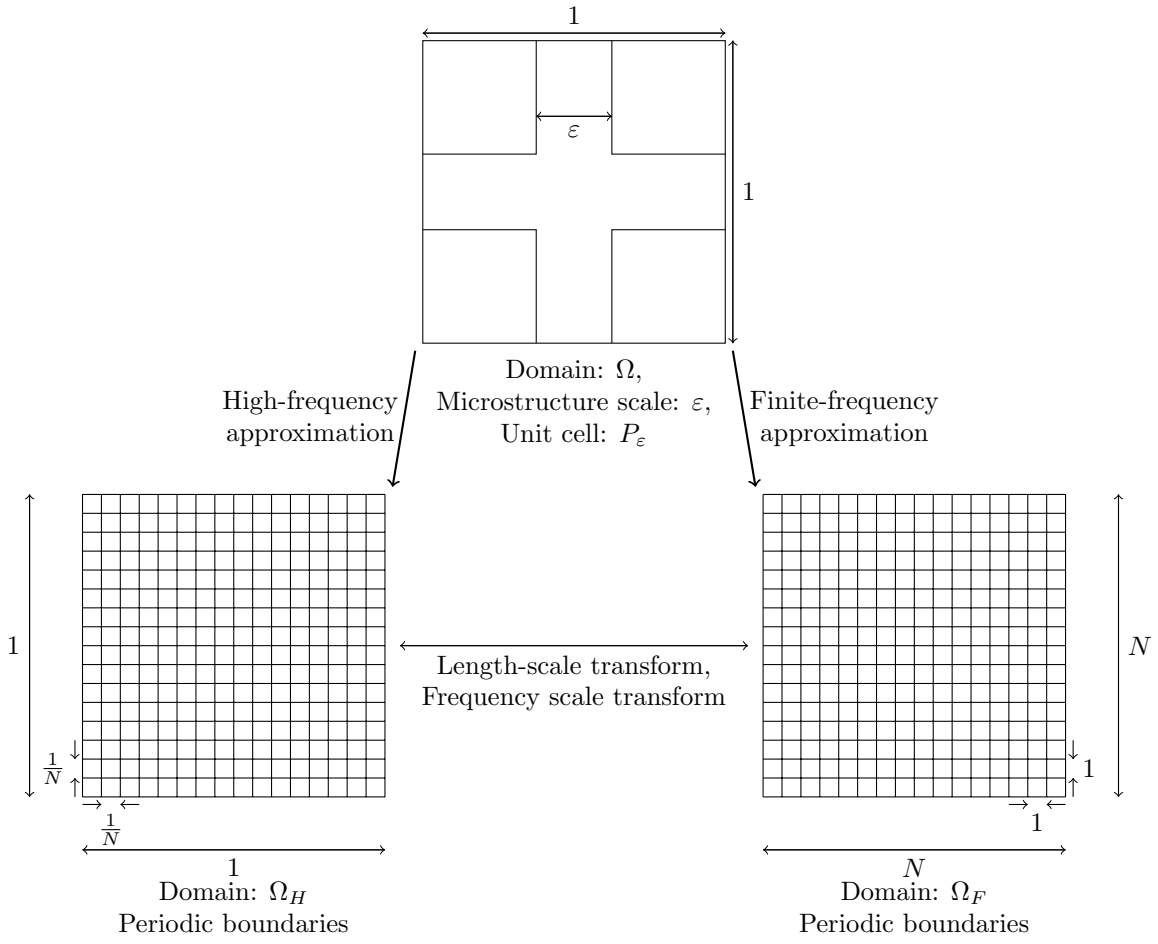

Figure 1.2: Illustration of the original, finite-frequency and high-frequency problems; their domains, and their relation to each other. This represents a 2D-system with period cell the unit square (the 2-dimensional analogue of the text).

[11] To illustrate what is meant by vertex- and edge-volume we can use the 2-dimensional examples in Figure 1.2 and

and $V^{(\mathrm{E})}$ determines the appropriate boundary conditions at the interior vertices of the graph, which ensure that the spectrum of the singular structure problem coincides with the limit σ_{ε,N^*} as $\varepsilon \to 0$. To describe each case, we adopt the language of [7]:

- Fast-Decaying $V^{(\mathrm{V})}$: If $V^{(\mathrm{V})}$ decays significantly faster than $V^{(\mathrm{E})}$ then at the interior vertices we impose continuity of the solution (coming from each of the edges into the vertex) and a classical Kirchhoff condition. A classical Kirchhoff condition imposes that the sum of the derivatives[12] of the edge solutions into the vertex (signed according to direction into or out of the vertex) be equal to 0:

$$\sum_{e_j \in E \text{ connects to } v_k} \mathrm{dir}\left(u_j\right) u_j'\left(v_k\right) = 0$$

  where $\mathrm{dir}\left(u_j\right)$ stands-in for effect of the directing the derivatives into v_k.

- Slow-Decaying $V^{(\mathrm{V})}$: If $V^{(\mathrm{V})}$ decays slower than $V^{(\mathrm{E})}$, the edges are essentially independent from the vertices and the structure effectively "breaks down". We obtain a Dirichlet problem on each edge-interval and vertex-domain, and the resulting spectrum is the union of the spectra of the decoupled problems. This is referred to as "Dirichlet decoupling".

- Boarderline Case: If $V^{(\mathrm{V})}$ decays at the same rate as $V^{(\mathrm{E})}$, then we obtain conditions of continuity and non-classical Kirchhoff conditions at the interior vertices. These non-classical conditions involve the spectral parameter ω^2, and have the form

$$\sum_{e_j \in E \text{ connects to } v_k} \mathrm{dir}\left(u_j\right) u_j'\left(v_k\right) = \omega^2 u\left(v_k\right).$$

  The value of the solution $u\left(v_k\right)$ exists due to the condition of continuity that is applied at each interior vertex. This non-classical Kirchhoff condition can give rise to "band-gap" phenomena, discussed shortly.

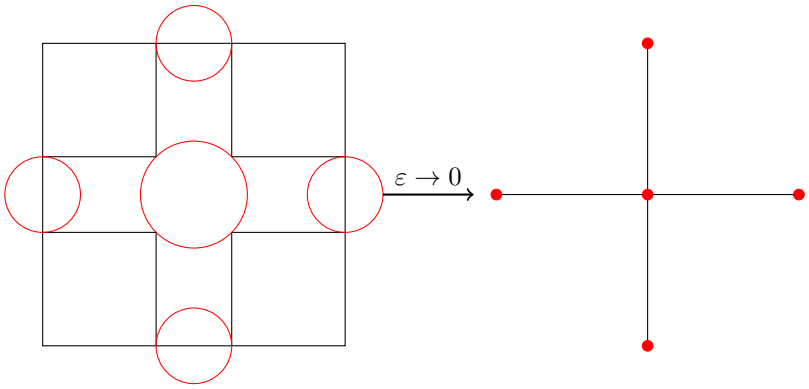

Figure 1.3: Illustration of a graph problem obtained by letting $\varepsilon \to 0$, the mcirostructure on the left is represented by the graph on the right. Red circles represent regions where connections and junctions in the microstructure occur, which become nodes in the graph representation.

Figure 1.3: each edge has $V^{(\mathrm{E})}$ equal to the volume of the arms of the cross, whose width is ε and so $V^{(\mathrm{E})} \propto \varepsilon$. The vertices (at the centre of the cross and the edges) have radius proportional to ε, and so $V^{(\mathrm{V})} \propto \varepsilon^2$ - note that if we were in 3-dimensions the volumes would scale at different rates.

[12]Strictly, this sum may also be weighted if the setup of the original problem is correct. However for our purposes this is unnecessary.

The sequence of problems $\mathcal{P}_{0,N}$ leads us (as $N \to \infty$) to a periodic singular structure in the whole of $\mathbb{R}^d$, each spectrum $\sigma_{0,N}$ being a sequence of points on the positive real axis. These spectra "fill up" the positive real axis, producing a spectrum which is a union of intervals in $(0, \infty)$ and which coincides with the spectrum of a periodic singular-structure problem on the whole of $\mathbb{R}^d$ [7], [8]. This raises the concept of a band-gap spectrum, a spectrum which can be represented as a (potentially infinite) union of (disjoint) intervals in the positive real axis, but which does not fill the entirety of $(0, \infty)$.

One can take the limits $N \to \infty$ and $\varepsilon \to 0$ simultaneously, and in such a way that there exists $N\varepsilon^\alpha \to \gamma \in (0, \infty)$ (for some $\alpha, \gamma \in (0, \infty)$). The importance of this double limit; besides mathematical curiosity in the properties of the result, is that certain materials may be poorly approximated in the other regimes - and photonic crystals fall into this category. The resulting limit of the spectra $\sigma_{\varepsilon,N}$ is then determined by a singular-structure problem, posed in the whole of $\mathbb{R}^d$, with period cell of side 1 and with vertex boundary conditions determined by the vetex- and edge-volume scaling. Crucially however, this problem does not represent a periodic singular-structure in the whole of $\mathbb{R}^d$, but rather the original thin-structure problem posed in Ω. This provides us with a method of determining the spectrum of thin-structure problems by analysis of thin-structure problems; such problems may be more open to mathematical analysis (which we will demonstrate with the examples in Chapter 2) and also bypass the computational complexities of numerical solvers for problems in multiple dimensions. This also means that certain periodic, thin-structure materials may have spectra composed of sub-intervals of $(0, \infty)$, separated by gaps of increasing length (see Section 2.2). This idea will be central to our application of the preceding theory to PCFs as the band gap spectrum determines which frequencies of light can (or cannot) propagate in the microstructure. If the remainder of the domain is interpreted as vacuum (or any dielectric material in the event of a solid-core fibre) then the band gaps determine the frequencies at which the fibre can be used to transmit information, we will develop this further in Chapter 4.

1.5 Report Outline

This report intends to demonstrate how the mathematical concepts that we introduced above can assist the development of PCFs. Chapter 2 aims to demonstrate the theory introduced in Section 1.4 by means of explicit examples. These examples will focus on the scalar-divergence equation $-\nabla^2 u = \omega^2 u$ on a suitable periodic domain $\Omega \subset \mathbb{R}^2$ with microstructure in each unit cell. It will explicitly determine the spectrum of the problem in the fast-decaying vertex volume case, demonstrating that the effective problem represents a homogenised medium. Additionally there will be a presentation of a problem in the borderline case (of vertex scaling) which will demonstrate the concepts of spectral band gaps, and provide some analysis which proves that this particular spectrum is composed of unions of sub-intervals of the positive real axis. Chapter 3 will use numerical techniques (based around the Finite Element Method) to analyse the spectra of a sequence of thin structure problems in the limit $N \to \infty$, $\varepsilon \to 0$ with $N\varepsilon^\alpha \to \gamma \in (0, \infty), \alpha > 0$. The purpose of this section will be to demonstrate the technicalities of numerical approaches to this problem, to link up with the demonstrations of Chapter 2, and to reinforce the earlier claim of the spectrum of the effective problem being the limit of the sequence of spectra $\sigma_{\varepsilon,N}$. The report will conclude with Chapter 4, which will develop the ideas presented thus far in the context of electromagnetics. This will include how to physically interpret (and setup) the domains that problems are posed in; a discussion of how to adapt the previous methods to suit the more complex system of Maxwell equations, how such a model would fit into the broader set of existing models for PCFs, and speculate on further generalisations that can be made to the model and how these might be implemented. This will culminate in a summary of the ideas that have been presented and a proposal for studying PCFs using the theory and methods discussed in the report.

Chapter 2

Graph Problems and Spectra

In this chapter we illustrate some of the concepts relating to singular-structure (graph) problems. This is in view of demonstrating the theory presented in Chapter 1; but also to demonstrate the concept of a band-gap spectrum, and to set the stage for Chapter 3 (which will explore the eigenvalue problem on a domain which in the limits $N \to \infty, \varepsilon \to 0$ reduces to the problems in this chapter). With this in mind, we will derive the spectrum of a periodic singular-structure occupying all of $\mathbb{R}^2$, and numerically examine the limit of the spectra of singular-structure problems on domains of size N in the fast-decaying vertex case (Section 1.4). In the borderline case, some analysis is performed which justifies the description of the spectrum as a series of "spectral bands".

Our examples will revolve around the graph $\mathbb{G}$ whose periodic unit cell is illustrated in Figure 2.1. $\mathbb{G}$ is chosen because it's structure is identical to that of the effective singular-structure problem for the thin-structure problem discussed in Chapter 3. $\mathbb{G}$ consists of 5 vertices $V = \{v_1, v_2, v_3, v_4, v_5\}$ and 4 edges $E = \{e_{13}, e_{35}, e_{23}, e_{34}\}$, and is embedded in $\mathbb{R}^2$. We identify each vertex with a point in $\mathbb{R}^2$ (cf Section 1.2)

$$\mathbf{v}_1 = \left(\frac{1}{2}, 0\right), \mathbf{v}_2 = \left(0, \frac{1}{2}\right) \mathbf{v}_3 = \left(\frac{1}{2}, \frac{1}{2}\right), \mathbf{v}_4 = \left(1, \frac{1}{2}\right), \mathbf{v}_5 = \left(\frac{1}{2}, 1\right),$$

and identify the edges with intervals

$$e_{13} = I_1 = \left[0, \frac{1}{2}\right], \quad e_{35} = I_2 = \left[\frac{1}{2}, 1\right], \quad e_{23} = I_3 = \left[0, \frac{1}{2}\right], \quad e_{34} = I_4 = \left[\frac{1}{2}, 1\right],$$

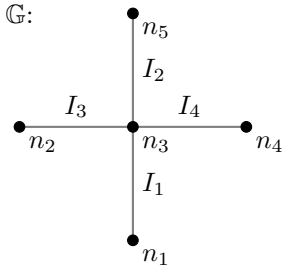

Figure 2.1: The unit cell of the graph $\mathbb{G}$; embedded in $\mathbb{R}^2$ and periodic in 2 dimensions.

where we adopt a single index for the intervals for later simplicity. Denote the solution to a particular ODE posed along an edge with interval I_j as u_j, so that the solution on the whole graph can be given by its associated set of edge solutions $\{u_j : I_j \to \mathbb{C}\}$.

Throughout this section we will be looking at the spectrum of the scalar-divergence operator

$$\mathcal{A}u = -\nabla^2 u,$$

on a periodic graph (hence the effective problem for a thin-structure problem in a periodic domain). We will work in the low-frequency framework, and shall take $\mathbb{G}$ as the unit cell of the singular-structure. Introducing the length-scale N we let $\mathbb{G}_N$ be the square domain formed from N^2 copies and translations of $\mathbb{G}$ (schematically illustrated in Figure 2.2(a)). We introduce a labelling system for each periodic cell (copy of $\mathbb{G}$) using the location of the bottom-left (south-west) corner of the unit cell — hence the cell with label (x', y') is the cell that is contained in $[x', x'+1] \times [y', y'+1]$. For a cell with label (x', y') we denote the vertices with $v_{x',y',k}$ and edges with $e_{x',y',kl}$[1] and maintain the local numbering system of $\mathbb{G}$ (illustrated in Figure 2.2(b)). Hence the edges are identified with the intervals $I_{x',y',j}$:

$$e_{x',y',13} = I_{x',y',1} = \left[y', y' + \frac{1}{2}\right], \quad e_{x',y',35} = I_{x',y',2} = \left[y' + \frac{1}{2}, y' + 1\right],$$
$$e_{x',y',23} = I_{x',y',3} = \left[x', x' + \frac{1}{2}\right], \quad e_{x',y',34} = I_{x',y',4} = \left[x' + \frac{1}{2}, x' + 1\right],$$

and we denote the solution along an edge associated with interval $I_{x',y',j}$ as $u_{x',y',j}$. We also number the cells from 0 through to $N^2 - 1$, along the x then y directions (which will be useful later, when we need to construct linear systems on $\mathbb{G}_N$). This construction of $\mathbb{G}_N$ results in vertices "on top of" one another: in an $N = 2$ for example, system the vertices $v_{0,0,4}$ and $v_{1,0,2}$ are both positioned at $\left(1, \frac{1}{2}\right)$, and so we identify these vertices with each other. Finally, we refer to the vertices that lie on any of the lines $x = 0, x = N, y = 0, y = N$ as "hanging vertices" or and all other vertices are called "interior vertices". At the hanging vertices we impose the periodicity conditions, identifying the nodes at $x = 0$ with those as $x = N$ and similarly for the y-direction. The interior nodes will have boundary conditions imposed at them, which is determined by the scaling of the vertex and edge volumes, $V^{(\mathrm{V})}$ and $V^{(\mathrm{E})}$ according to Section 1.4. Finally (in a slight abuse of notation) we let $\mathbb{G}_\infty$ denote the singular-structure that occupies the whole of $\mathbb{R}^2$, with unit cell $\mathbb{G}$. Note that the previous labelling convention for cell (x', y') are still applicable in this case.

Finally, we include a brief analysis of the general eigenvalue-eigenfunction problem of the form

$$-\left(\frac{\mathrm{d}}{\mathrm{d}x} + i\phi\right)^2 v(x) = \omega^2 v(x), \quad x \in I$$
$$\Leftrightarrow \frac{\mathrm{d}^2}{\mathrm{d}^2 x} v + 2i\phi \frac{\mathrm{d}}{\mathrm{d}x} v - \phi^2 v = -\omega^2 v,$$

for some interval $I \subset \mathbb{R}$ and function to be determined $v(x)$, with ϕ, ω constants (hence the $2i\phi\dfrac{\mathrm{d}}{\mathrm{d}x}v$ term as opposed to the more general $\dfrac{\mathrm{d}}{\mathrm{d}x}(i\phi v) + i\phi\dfrac{\mathrm{d}}{\mathrm{d}x}v$). The function $v = e^{\lambda x}$ solves this ODE, provided that

$$\lambda^2 + 2i\phi\lambda + (\omega^2 - \phi^2) = 0,$$
$$\implies \lambda = -i\phi \pm i\omega,$$

[1] With $k, l \in \{1, ..., 5\}$ and $j \in \{1, ..., 4\}$.

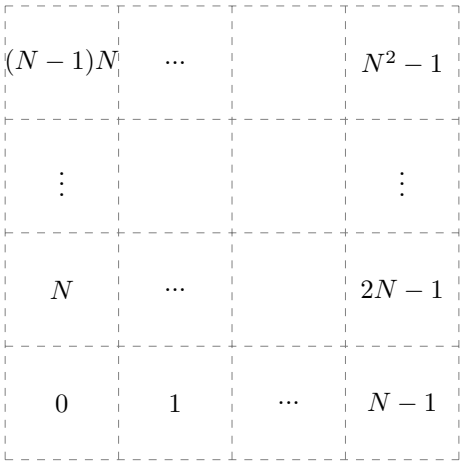

(a) The arrangement of the peridoic cells in the domain. Each cell is a translated copy of $\mathbb{G}$, and they are arranged in an $N \times N$ square. The labelling of the components of the unit cell is shown to the right.

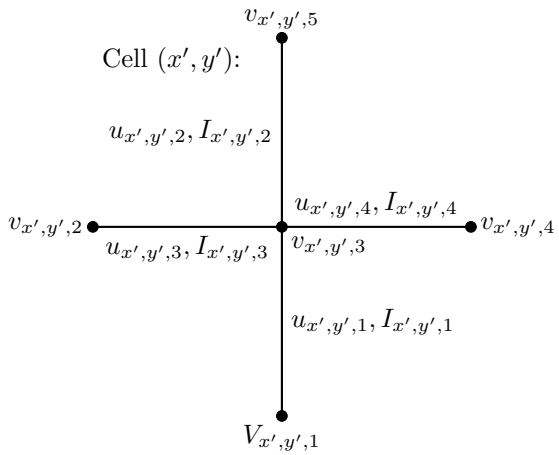

(b) Local labelling of nodes and solution pieces within a unit cell (x', y')

Figure 2.2: The domain $\mathbb{G}_N$. Periodicity is imposed at the hanging vertices, and the conditions on the interior vertices are determined by the relative scaling of $V^{(\mathrm{V})}$ and $V^{(\mathrm{E})}$.

and hence we obtain

$$v(x) = e^{-i\phi x}\left(c^{(1)}e^{i\omega x} + c^{(2)}e^{-i\omega x}\right), \tag{2.1}$$

for constants $c^{(1)}, c^{(2)} \in \mathbb{C}$ which are determined by the boundary conditions at the endpoints of I (at the vertices, for our cases). This will be the form of the solutions along the edges u_j, and so we provide a corresponding subscript $c_j^{(1)}, c_j^{(2)} \in \mathbb{C}$ for the constants to be determined by the vertex conditions.

2.1 Fast-Decaying Vertex Case

We begin with an example in the fast-decaying vertex case, which results in us obtaining continuity and (classical) Kirchhoff conditions at the interior nodes. Using the Gelfand transform (Section 1.2) to analyse the spectrum of $\mathcal{A}$ posed in $\mathbb{G}_\infty$ requires introducing the quasi-momentum θ_1 corresponding to the periodicity in the x-axis, and θ_2 that in the y-axis. As the unit cell of $\mathbb{G}_\infty$ is $\mathbb{G}$ which is contained in the unit square, the range of both quasi-momentum is $\theta_1, \theta_2 \in [-\pi, \pi)$. We now look to analyse each of the operators $\mathcal{A}^{(\theta_1,\theta_2)}$, and will obtain the spectrum of $\mathcal{A}$ by taking the union of the spectra of $\mathcal{A}^{(\theta_1,\theta_2)}$ over θ_1 and θ_2. As the edges of $\mathbb{G}$ are parallel to the co-ordinate axes, the operator $\mathcal{A}^{(\theta_1,\theta_2)}$ reduces to the operation $-\left(\frac{\mathrm{d}}{\mathrm{d}x} + i\theta_1\right)^2$ on edges parallel to the x-axis and $-\left(\frac{\mathrm{d}}{\mathrm{d}x} + i\theta_2\right)^2$ on those parallel to the y-axis[2]. Working on $\mathbb{G}$ means that we only have one interior vertex v_3, at which we have continuity and classical Kirchhoff conditions. Periodicity of the solution and first-derivative

[2]In general the graph may have diagonal edges, and so the effect of the quasi-momentum on the operator along the edges is slightly more complex.

across $v_1 \leftrightarrow v_5$ and $v_2 \leftrightarrow v_4$ is also imposed.

Compiling this information, we arrive at the system

$$-\left(\frac{\mathrm{d}}{\mathrm{d}x}+i\theta_1\right)^2 u_1(x)=\omega^2 u_1(x), \qquad x\in I_1 \tag{2.2a}$$

$$-\left(\frac{\mathrm{d}}{\mathrm{d}x}+i\theta_1\right)^2 u_2(x)=\omega^2 u_2(x), \qquad x\in I_2 \tag{2.2b}$$

$$-\left(\frac{\mathrm{d}}{\mathrm{d}x}+i\theta_2\right)^2 u_3(x)=\omega^2 u_3(x), \qquad x\in I_3 \tag{2.2c}$$

$$-\left(\frac{\mathrm{d}}{\mathrm{d}x}+i\theta_2\right)^2 u_4(x)=\omega^2 u_4(x), \qquad x\in I_4 \tag{2.2d}$$

with the boundary conditions arising from continuity at v_3;

$$u_1\left(\frac{1}{2}\right)=u_2\left(\frac{1}{2}\right), \tag{2.2e}$$

$$u_1\left(\frac{1}{2}\right)=u_3\left(\frac{1}{2}\right), \tag{2.2f}$$

$$u_3\left(\frac{1}{2}\right)=u_4\left(\frac{1}{2}\right), \tag{2.2g}$$

from periodicity;

$$u_1(0)=u_2(1), \tag{2.2h}$$

$$u_3(0)=u_4(1), \tag{2.2i}$$

$$\left(\frac{\mathrm{d}}{\mathrm{d}x}+i\theta_1\right)u_1\Big|_0=\left(\frac{\mathrm{d}}{\mathrm{d}x}+i\theta_1\right)u_2\Big|_1, \tag{2.2j}$$

$$\left(\frac{\mathrm{d}}{\mathrm{d}x}+i\theta_2\right)u_3\Big|_0=\left(\frac{\mathrm{d}}{\mathrm{d}x}+i\theta_2\right)u_4\Big|_1, \tag{2.2k}$$

and from the classical Kirchhoff condition at v_3,

$$0=\sum_{j=1}^{4}(-1)^j\left(\frac{\mathrm{d}}{\mathrm{d}x}+i\theta_{\lceil j/2\rceil}\right)u_j\Big|_{\frac{1}{2}}, \tag{2.2l}$$

with $\lceil x\rceil$ denoting the ceiling function applied to x, which we use to give the Kirchhoff condition a succinct form. Note also the factor of $(-1)^j$ in the Kirchhoff condition, accounting for the direction of the derivative into v_3. Using the short analysis in this chapter's introduction, the edge solutions u_j have the form of (2.1),

$$u_j(x)=e^{-i\theta_{\lceil j/2\rceil}x}\left(c_j^{(1)}e^{i\omega x}+c_j^{(2)}e^{-i\omega x},\right)$$

for constant coefficients $c_j^{(k)}\in\mathbb{C}$ ($k\in\{1,2\}$) to be determined by the boundary conditions (2.2e)-(2.2l). Determining these constants amounts to solving the linear system $A_\infty(\omega)\,\mathbf{c}=0$; where $\mathbf{c}$ the

column vector of the coefficients (ordered by j then the superscript), and A_∞ the matrix

$$\begin{pmatrix}
e^{\frac{i\omega}{2}} & e^{-\frac{i\omega}{2}} & -e^{\frac{i\omega}{2}} & -e^{-\frac{i\omega}{2}} & 0 & 0 & 0 & 0 \\
e^{\frac{i(\omega-\theta_1)}{2}} & e^{-\frac{i(\omega+\theta_1)}{2}} & 0 & 0 & -e^{\frac{i(\omega-\theta_2)}{2}} & -e^{-\frac{i(\omega+\theta_2)}{2}} & 0 & 0 \\
0 & 0 & 0 & 0 & e^{\frac{i\omega}{2}} & e^{-\frac{i\omega}{2}} & -e^{\frac{i\omega}{2}} & -e^{-\frac{i\omega}{2}} \\
1 & 1 & -e^{i(\omega-\theta_1)} & -e^{-i(\omega+\theta_1)} & 0 & 0 & 0 & 0 \\
0 & 0 & 0 & 0 & 1 & 1 & -e^{i(\omega-\theta_2)} & -e^{-i(\omega+\theta_2)} \\
1 & -1 & -e^{i(\omega-\theta_1)} & e^{-i(\omega+\theta_1)} & 0 & 0 & 0 & 0 \\
0 & 0 & 0 & 0 & 1 & -1 & -e^{i(\omega-\theta_2)} & e^{-i(\omega+\theta_2)} \\
-e^{\frac{i(\omega-\theta_1)}{2}} & e^{-\frac{i(\omega+\theta_1)}{2}} & e^{\frac{i(\omega-\theta_1)}{2}} & -e^{-\frac{i(\omega+\theta_1)}{2}} & -e^{\frac{i(\omega-\theta_2)}{2}} & e^{-\frac{i(\omega+\theta_2)}{2}} & e^{\frac{i(\omega-\theta_2)}{2}} & -e^{-\frac{i(\omega+\theta_2)}{2}}
\end{pmatrix} \tag{2.3}$$

formed from the boundary condition equations. Those ω that correspond to eigenfrequencies are those for which we have $\det(A_\infty) = 0$, so that the vector $\mathbf{c} \neq \mathbf{0}$ and hence we obtain non-trivial solution u. With some calculation it can be shown that this requires

$$\begin{aligned}
0 = \sin(\omega)\,[& -2e^{-i\theta_1}e^{-i\theta_2}e^{2i\omega} \\
& + \left(e^{-i\theta_1}e^{-2i\theta_2} + e^{-2i\theta_1}e^{-i\theta_2} + e^{-i\theta_1} + e^{-i\theta_2}\right)e^{i\omega} \\
& - 2e^{-i\theta_1}e^{-i\theta_2}].
\end{aligned} \tag{2.4}$$

Note that the factor of $\sin(\omega)$ implies that $\omega = n\pi$ for $n \in \mathbb{N}$ is an eigenfrequency for all θ_1, θ_2. Otherwise, we can write the second factor in a more explicit form,

$$e^{i\omega} = \cos\left(\frac{\theta_1+\theta_2}{2}\right)\cos\left(\frac{\theta_1-\theta_2}{2}\right) \pm i\left(1-\cos^2\left(\frac{\theta_1+\theta_2}{2}\right)\cos^2\left(\frac{\theta_1-\theta_2}{2}\right)\right)^{\frac{1}{2}}. \tag{2.5}$$

If a particular ω satisfies (2.5) (for given θ_1, θ_2), then $\omega + 2n\pi$ also satisfies (2.5) for any $n \in \mathbb{N}$, and therefore the spectrum of the problem (2.2) can be fully described by only considering $\omega \in (0, 2\pi]$ and extending periodically. Recognising real and imaginary parts of both sides of (2.5), we can find explicit expressions for trigonometric functions of ω:

$$\cos(\omega) = \cos\left(\frac{\theta_1+\theta_2}{2}\right)\cos\left(\frac{\theta_1-\theta_2}{2}\right), \tag{2.6a}$$

$$\sin(\omega) = \pm\left(1-\cos^2\left(\frac{\theta_1+\theta_2}{2}\right)\cos^2\left(\frac{\theta_1-\theta_2}{2}\right)\right)^{\frac{1}{2}}. \tag{2.6b}$$

By use of the identity $\sin^2\phi + \cos^2\phi = 1$ it can be shown that ω satisfies (2.6a) if and only if ω satisfies (2.6b), so it is sufficient to use only one of these equations to determine values of ω. As $\theta_1, \theta_2 \in [-\pi, \pi)$ the right hand side of (2.6a) attains every value in the interval $(-1, 1]$ as θ_1 and θ_2 vary in this range; hence every $\omega \in (0, \pi) \cup (\pi, 2\pi)$ will be a solution to this equation for some (not necessarily unique) pair of (θ_1, θ_2). Combined with the earlier deduction that $\omega = n\pi$ is an eigenfrequency for all values of θ_1, θ_2, this implies that the union over θ_1, θ_2 of all eigenfrequencies ω is the interval $(0, 2\pi]$. Hence by the 2π-periodicity of the solutions for ω, the spectrum of $\mathcal{A}$ is the entire positive real line, $(0, \infty)$.

Next we consider the sequence of (finite-frequency approximation) problems $\mathcal{A}_N u = -\nabla^2 u$ for functions $u \in L^2(\mathbb{G}_N)$. Let σ_N denote the spectrum of $\mathcal{A}_N$ for each $N \in \mathbb{N}$. We can recycle the above analysis to determine σ_1, as by setting $\theta_1 = \theta_2 = 0$ we obtain the setup for the $N = 1$ problem. This provides the spectrum $\sigma_1 = \{n\pi \mid n \in \mathbb{N}\}$. For the other cases, we systematically associate each 1×1 cell of $\mathbb{G}_N$ with 8 boundary conditions. A cell (x', y') provides 3 equations from

continuity at the vertex $v_{x',y',3}$ and 1 equation from the Kirchhoff condition at the same vertex, which involve only arbitrary constants of solutions $u_{x',y',j}$ (that is, only edge solutions that belong to the cell itself). The other 4 conditions relate to other neighbouring cells at the edge vertices of the cell - we associate the conditions including the neighbouring cells to the "left" and "below". That is, we associate the matching conditions (continuity of solution and first derivative) at $v_{x',y',2} \leftrightarrow v_{x'-1,y',4}$ and $v_{x',y',1} \leftrightarrow v_{x',y'-1,5}$, replacing these with the appropriate periodic conditions in the event that $x' = 0$ or $y' = 0$. This gives us the $8N^2 \times 8N^2$ system $A_N(\omega)\,\mathbf{c}_N = \mathbf{0}$ where $\mathbf{c}_N$ is the vector of arbitrary constants of the edge solutions (now ordered by cell label, then j, then superscript) and A_N is the matrix for the linear system of equations, which has sparsity pattern as shown in Figure 2.3(a) thanks to the method of associating boundary conditions with each cell. $\det(A_N(\omega))$ is 2π-periodic in ω when N is odd, and π-periodic when N is even (one can deduce this from the form of the boundary conditions and the way ω appears in them). Additionally, the determinant is entirely imaginary for odd N, and entirely real for even N. Computations examining $\det(A_N(\omega))$ imply that $\omega = n\pi$ is a root of this quantity for every $N, n \in \mathbb{N}$; and furthermore each N produces $2N$ other roots for $\omega \in (0, 2\pi) \setminus \{\pi\}$, however this is hard to verify analytically due to the size of A_N. However it can be seen that the number of solutions for ω is increasing with N; and these are becoming increasing "dense" along the real line, as we expect due to our knowledge of the full-space problem. Some examples of $\det(A_N(\omega))$ are shown in Figure 2.3(b).

2.2 Borderline Case (Non-Classical Kirchhoff Condition)

Following the conclusion of Section 2.1, we now explore the borderline vertex-scaling case, and illustrate the concept of "spectral band gaps". Again we first consider the domain $\mathbb{G}_\infty$, and seek the spectrum of the operator $\mathcal{A}$; only this time consider ourselves in the borderline case and impose a non-classical Kirchhoff condition at the interior vertices. We introduce the quasi-momentum $\theta_1, \theta_2 \in [-\pi, \pi)$ and family of operators $\mathcal{A}^{(\theta_1,\theta_2)}$, and analyse a problem posed on (the unit cell) $\mathbb{G}$. We obtain a system analogous to (2.2) but with the Kirchhoff condition at v_3 replaced with the

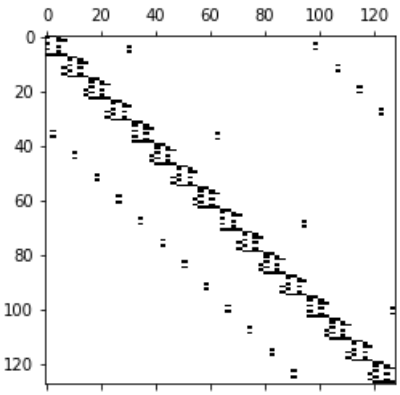

(a) Sparsity pattern of the matrix A_N, for $N = 4$. Entries that are not in the diagonal "blocks" correspond to conditions that involve multiple unit cells.

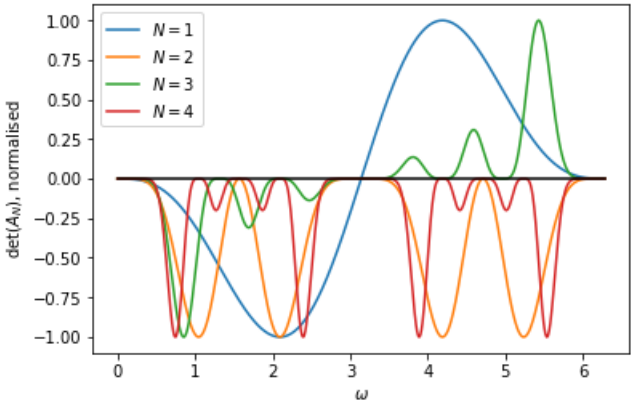

(b) The quantity $\det(A_N(\omega))$ over the range $(0, 2\pi)$, for $N = 1, 2, 3, 4$. Periodicity of the determinant can be seen. Note that values are normalised for each N to allow for visualisation.

Figure 2.3: The sparsity pattern of the matrix A_N (left) and the behaviour of it's determinant as a function of ω (right).

"non-classical Kirchhoff" condition

$$\alpha\omega^2 u(\mathbf{v}_3) = \sum_{j=1}^{4} (-1)^j \left(\frac{\mathrm{d}}{\mathrm{d}x} + i\theta_{\lceil j/2 \rceil}\right) u_j\Big|_{\frac{1}{2}},$$

where $u(\mathbf{v}_3)$ is the value of the solution at the central vertex (which exists due to the condition of continuity at v_3) and α a constant which is related to $V^{(\mathrm{V})}$. Again we can express the resulting system as a matrix equation $A_\infty(\omega)\,\mathbf{c} = \mathbf{0}$[3]. Again we seek those ω which solve $\det(A_\infty(\omega)) = 0$, which can be shown to be those ω which satisfy the equation

$$0 = \frac{1}{2} i\alpha\omega \left(e^{2i\omega} - 1\right) \left(\frac{\alpha\omega}{4}\sin(\omega) + \cos(\omega) - \cos\left(\frac{\theta_1 - \theta_2}{2}\right)\cos\left(\frac{\theta_1 + \theta_2}{2}\right)\right).$$

This means that $\omega = n\pi$ for any $n \in \mathbb{N}_0$ is a solution, due to the factor of $e^{2i\omega} - 1$. Other values for ω do not have a closed form and must be determined numerically from the equation

$$\frac{\alpha\omega}{4}\sin(\omega) + \cos(\omega) = \cos\left(\frac{\theta_1 - \theta_2}{2}\right)\cos\left(\frac{\theta_1 + \theta_2}{2}\right), \tag{2.7}$$

however we can make some deductions about the spectrum of $\mathcal{A}$ analytically. For ease of reference we denote the left hand side of (2.7) by the function

$$\begin{aligned} \Xi(\omega) : (0,\infty) &\to \mathbb{R}, \\ \omega &\mapsto \frac{\alpha\omega}{4}\sin(\omega) + \cos(\omega), \end{aligned}$$

and the right hand side by

$$\begin{aligned} \Psi(\theta_1,\theta_2) : [-\pi,\pi)^2 &\to \mathbb{R}, \\ (\theta_1,\theta_2) &\mapsto \cos\left(\frac{\theta_1 - \theta_2}{2}\right)\cos\left(\frac{\theta_1 + \theta_2}{2}\right). \end{aligned}$$

Ψ is continuous in both it's variables, and is bounded between (and attains) -1 and 1 hence achieves every value in the interval $[-1,1]$. For a given (θ_1,θ_2), (2.7) has constant right-hand side and is equivalent to seeking a level set of Ξ. Hence the spectrum (the union over all θ_1,θ_2 of eigenfrequencies ω) are those ω for which $\Xi(\omega)$ lies in the image of Ψ, namely those ω for which

$$-1 \leq \frac{\alpha\omega}{4}\sin(\omega) + \cos(\omega) \leq 1. \tag{2.8}$$

One can visualise the function Ξ in Figure 2.4(a), and the corresponding spectral values that are obtained in Figure 2.4(b). As can be seen, the spectral values appear to form a disjoint set of intervals, the "spectral bands" or simply "bands".

Going further than visual inspection, it can be proved that the operator $\mathcal{A}$ has a genuine band-gap spectrum - a union of "(spectral) bands" I_n for $n \in \mathbb{N}$. This follows from some analysis of Ξ, for which we need the following result:

Lemma 2.2.1 (Critical Points of Ξ)**.** *Let $n \in \mathbb{N}$. Then Ξ has at most one critical point in the interval $((n-1)\pi, n\pi)$.*
Equivalently, Ξ' has at most one root in the interval $((n-1)\pi, n\pi)$.

[3]One can make a choice of $u(\mathbf{v}_3)$ as any of the edge solutions u_j evaluated at $\frac{1}{2}$.

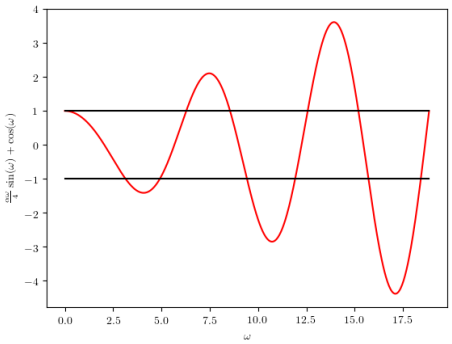

(a) The function Ξ plotted for $0 \leq \omega \leq 6\pi$. The black lines are positioned at -1 and 1 on the y-axis, so whenever the red line lies between the black lines the corresponding ω is an eigenfrequency. One can see visually that the eigenfrequencies are separated into disjoint intervals.

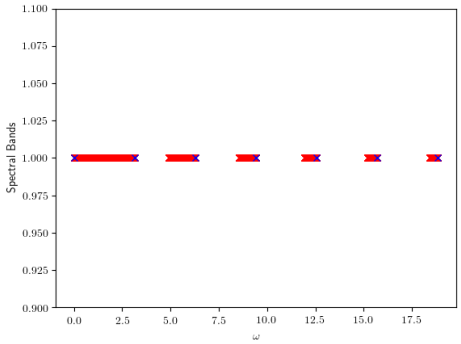

(b) Illustration of the spectral bands in ω that arise from the 2D graph problem with a non-classical Kirchhoff condition at the central vertex. Blue crosses correspond to eigenfrequencies at $\omega = n\pi$ for $n \in \mathbb{N}_0$. Note that the length of successive bands is decreasing, and each $n\pi$ is the right-endpoint of a band.

Figure 2.4: The relation between the function Ξ and the spectral values ω.

Proof. Note that

$$\Xi'(\omega) = \frac{\alpha\omega}{4}\cos(\omega) + \left(\frac{\alpha}{4} - 1\right)\sin(\omega). \tag{2.9}$$

In the case $\alpha = 4$, (2.9) reduces to $\Xi'(\omega) = \omega\cos(\omega)$. As $\omega > 0$, roots can only occur when $\cos(\omega) = 0$, which occurs precisely once for $\omega \in ((n-1)\pi, n\pi)$ - at $\omega = \left(n - \frac{1}{2}\right)\pi$.
Otherwise we express Ξ' using a single trigonometric function,

$$\Xi'(\omega) = \frac{1}{4}\left(\alpha^2\left(\omega^2+1\right) - 8\alpha + 16\right)^{\frac{1}{2}} \sin\left(\omega + \tan^{-1}\left(\frac{\alpha\omega}{\alpha-4}\right)\right). \tag{2.10}$$

Now

$$\begin{aligned} \alpha^2\left(\omega^2+1\right) - 8\alpha + 16 &\leq 0, \\ \Leftrightarrow \omega^2 &\leq -\frac{1}{\alpha^2}(\alpha-4)^2, \end{aligned}$$

which posthumously justifies the use of the square-root, and also implies that $\Xi' = 0$ only when the sine factor is equal to zero. Now note that $\tan^{-1}\left(|\frac{\alpha}{\alpha-4}|\omega\right)$ is bounded below by 0 and above by $\frac{\pi}{2}$. Hence, in the case when $\alpha > 4$, $|\frac{\alpha}{\alpha-4}| = \frac{\alpha}{\alpha-4}$ and so

$$(n-1)\pi < \omega + \tan^{-1}\left(|\frac{\alpha}{\alpha-4}|\omega\right) < \left(n+\frac{1}{2}\right)\pi,$$

and over the interval $\left((n-1)\pi, \left(n+\frac{1}{2}\right)\pi\right)$, the sine function has precisely one root. Hence Ξ' as at most one root for $\omega \in ((n-1)\pi, n\pi)$, in this case. In the case $\alpha < 4$, we simply note that

$\tan^{-1}\left(\frac{\alpha\omega}{\alpha-4}\right) = -\tan^{-1}\left(|\frac{\alpha}{\alpha-4}|\omega\right)$, hence

$$\left(n-1-\frac{1}{2}\right)\pi < \omega - \tan^{-1}\left(|\frac{\alpha}{\alpha-4}|\omega\right) < n\pi,$$

and over the interval $\left(\left(n-1-\frac{1}{2}\right)\pi, n\pi\right)$ the sine function again has precisely one root; hence Ξ' has at most one root in $\omega \in ((n-1)\pi, n\pi)$, which concludes all cases and provides the result. □

Knowledge of the critical points of Ξ allows us to deduce that the spectrum is a union of intervals (justifying the use of the term "band"), with each interval containing exactly one multiple of π at it's right endpoint.

Proposition 2.2.2 (Spectral Bands, $n \geq 2$)**.** *For each $n \geq 2$ with $n \in \mathbb{N}$, there exists a $c_n \in ((n-1)\pi, n\pi)$ such that*

1. *$|\Xi| \leq 1$ on the interval $I_n := [c_n, n\pi]$,*
2. *$|\Xi| > 1$ on the interval $((n-1)\pi, c_n)$, and*
3. *I_n is the largest interval containing $n\pi$ on which $|\Xi| \leq 1$.*

Proof. We first assume that n is even. Then by direct computation we can find that

$$\Xi((n-1)\pi) = -1, \quad \Xi(n\pi) = 1,$$
$$\Xi'((n-1)\pi) < 0, \quad \Xi'(n\pi) > 0.$$

As Ξ' is continuous and changes sign over $[(n-1)\pi, n\pi]$, it has at least one root (by the Intermediate Value Theorem) in the interior of this interval. Combined with the result from Lemma 2.2.1, it has precisely one root in this interval. Hence Ξ has exactly one critical point in this interval. Furthermore, as $\Xi'((n-1)\pi) < 0$ there exists some $\delta > 0$ such that $\Xi(\omega) < \Xi((n-1)\pi) = -1$ for all $\omega \in ((n-1)\pi, (n-1)\pi + \delta)$. But Ξ is continuous and $\Xi(n\pi) = 1$, and thus Ξ must cross -1 again, at a point $c_n \in [(n-1)\pi + \delta, n\pi)$. Hence over the interval $((n-1)\pi, c_n)$ we have $\Xi < -1$, with $\Xi = -1$ at $(n-1)\pi$ and c_n (in particular, $|\Xi| > 1$). This implies that Ξ has a critical point in this interval, which by the above reasoning is it's only critical point in $((n-1)\pi, n\pi)$. Hence the choice of c_n is unique, and furthermore $\Xi \leq 1$ on $(c_n, n\pi)$ (were this not the case, this would imply Ξ had additional critical points to allow for "turning back" on itself), so we have that $-1 \leq \Xi \leq 1$ on $I_n := [c_n, n\pi]$. It remains to show that I_n is the largest such interval containing $n\pi$; and by the argument just concluded cannot extend the left endpoint of I_n. As for the right endpoint, $n\pi$ itself; we note that $\Xi'(n\pi) > 0$ here and $\Xi(n\pi) = 1$, hence there exists some $\varepsilon > 0$ such that $\Xi > 1$ on $(n\pi, n\pi + \varepsilon)$. Hence, we cannot extend the right endpoint either, and the result holds.
For the case when n is odd, an analogous argument holds, with reversed inequalities and similar reasoning. □

The case when $n = 1$ is separate because this case requires an understanding of the behaviour of Ξ near 0. For the analysis that follows it is convenient to temporarily extend the domain of Ξ to the other side of 0, say to $(-\frac{1}{2}, \infty)$, so that we can use arguments based on properties of Ξ and it's derivatives at 0 (without formally introducing one-sided derivatives and the like).

Proposition 2.2.3 (Spectral Band, $n = 1$)**.** *For consistency, we use similar notation to Proposition 2.2.2.*

1. *If $\alpha \leq 2$, then the interval $I_1 := (0, \pi]$ is the largest interval which contains π and on which $|\Xi| \leq 1$.*

2. *If $\alpha > 2$, there exists a $c_1 \in (0, \pi)$ such that the interval $I_1 := [c_1, \pi]$ is the largest interval which contains π and on which $|\Xi| \leq 1$, and $|\Xi| > 1$ on $(0, c_1)$.*

Note that the difference between cases is very subtle, namely that if $\alpha \leq 2$ then $c_1 = 0$ and I_n is half-open on the left; otherwise the conclusion is the same as in Proposition 2.2.2.

Proof. We begin by evaluating Ξ at π and 0:

$$\begin{aligned} \Xi(\pi) = -1, \quad \Xi'(\pi) < 0, \\ \Xi(0) = 1, \quad \Xi'(0) = 0. \end{aligned}$$

Like Proposition 2.2.2, the properties of Ξ and Ξ' at π lead to the conclusion that any interval which we seek must have right endpoint π. Unlike the $n \geq 2$ cases, $\Xi'(0) = 0$ so we cannot repeat the argument of Proposition 2.2.2 as we required knowledge of how the derivative behaved, which informed behaviour of Ξ. Instead, we turn to the second derivative of Ξ at 0, which is

$$\Xi''(0) = \frac{\alpha}{2} - 1.$$

Case $\alpha < 2$: In this case $\Xi'' < 0$ and so Ξ has a local maximum at 0. Hence there exists an $\varepsilon > 0$ such that $\Xi < 1$ on $(-\varepsilon, \varepsilon)$, in particular $\Omega < 1$ on $(0, \varepsilon)$. We now establish that $\Xi < 1$ on all of $(0, \pi)$ by contradiction: if there existed a $d \in (0, \pi)$ where $\Xi > 1$, Ξ must have a critical point between $(0, d)$ (to "turn around" from the maximum at 0), and must also intersect 1 at some $d_- \in (\varepsilon, d)$. However continuity of Ξ between d and π implies that Ξ intersects 1 again at $d_+ \in (d, \pi)$. Hence we have $d_- < d < d_+$ and also $\Xi(d_-) < \Xi(d) > \Xi(d_+)$ which implies the existence of a second critical point in (d_-, d_+), contradicting Lemma 2.2.1 and giving us that $\Xi < 1$ on all of $(0, \pi)$. We can also establish that $\Xi > -1$ on all of $(0, \pi)$: if if there existed a $d \in (0, \pi)$ where $\Xi < -1$, there exists a $d_- \in (0, d)$ where $\Xi(d_-) = -1$. However $\Xi(\pi) = -1$ so Ξ has a critical point in the interval (d_-, π), because $\Xi(d_-) > \Xi(d) < \Xi(\pi)$ this is a local minimum. Without loss of generality, we can say that the local minimum occurs at d (simply by changing labels of points). Now there exists a $\delta > 0$ such that $\Xi' > 0$ on $(d, d + \delta)$ as d is a local minimum; but $\Xi'(\pi) < 0$ so by continuity of Ξ' it has a root in (d, π), thus requiring existence of two roots of Ξ' in $(0, \pi)$ contradicting Lemma 2.2.1. Hence we have that $|\Xi| < 1$ on $(0, \pi)$, combined with $\Xi(\pi) = -1$ we have found that the spectral band $I_1 = (0, \pi]$.
Case $\alpha > 2$: In this case $\Xi'' > 0$ and so Ξ has a local minimum at 0. Hence there exists an $\varepsilon > 0$ such that $\Xi > 1$ on $(-\varepsilon, \varepsilon)$, in particular $\Xi > 1$ on $(0, \varepsilon)$. Continuity of Ξ then implies that there exists a $c_1 \in (\varepsilon, \pi)$ such that $\Xi(c_1) = 1$. This also means that Ξ must have a local maximum between $(0, c_1)$, which is it's only critical point in $(0, \pi)$ by Lemma 2.2.1. Thus we can establish that $-1 \leq \Xi \leq 1$ on $[c_1, \pi]$, as if this is not the case a second critical point for Ξ must exist (see the argument in Proposition 2.2.2) and that $|\Xi| > 1$ on $(0, c_1)$. Hence $I_1 = [c_1, \pi]$ for $c_1 \in (0, \pi)$.
Case $\alpha = 2$: Although the conclusion for this case is the same as that for the $\alpha < 2$ case, different reasoning is required as in this case $\Xi''(0) = 0 = \Xi'''(0)$. We do find that $\Xi^{(4)}(0) < 0$, which implies that Ξ'' has a local maximum at 0. Hence there exists an $\varepsilon > 0$ such that $\Xi''(\omega) < \Xi''(0) = 0$ for all $\omega \in (-\varepsilon, \varepsilon)$. Now applying the Mean Value Theorem to Ξ' between $(-\varepsilon, 0)$, we find that there exists some $d \in (-\varepsilon, 0)$ such that $\Xi''(d) = \frac{1}{\varepsilon}\Xi'(\varepsilon)$. But $d \in (-\varepsilon, 0)$ and $\varepsilon > 0$ hence $\Xi'(\varepsilon) < 0$. Ξ' is also an odd function, so $\Xi'(-\varepsilon) < 0$ and hence

$$\Xi'(-\varepsilon) < 0 < \Xi'(\varepsilon).$$

This also holds for any positive $\varepsilon^* < \varepsilon$ (the Mean Value Theorem is applied on $(-\varepsilon^*, 0)$ instead); thus Ξ has a point of inflection at 0, and because $\Xi' < 0$ on $(0, \varepsilon)$, we have that there exists some $\delta > 0$ such that $\Xi < 1$ on $(0, \delta)$. We then revert to the previous analysis of the critical points to deduce that $|\Xi| < 1$ on all of $(0, \pi)$, and hence obtain the result. □

Proposition 2.2.2 and Proposition 2.2.3 show that the spectral bands are all intervals, and a bijection exists from $\mathbb{N}$ to the set of spectral bands $\{I_n \mid n\pi \in I_n\}$. In addition the spectral bands are disjoint; the n^{th} band terminates at $n\pi$, and all bands are closed intervals, unless $\alpha \leq 2$ in which case the $n = 1$ band is open on the left with left endpoint 0. This is an important characteristic of the spectrum which we will revisit when we look to take a numerical approach at the corresponding thin-structure problem in Chapter 3.

2.3 Summary

The problems we have considered in this chapter demonstrate how the theory of Section 1.2 and Section 1.4 can be applied to singular-structures, to produce information about the spectrum of the operator we are concerned with. The concept of a band-gap spectrum is important to an application of this theory in the context of PCFs, as a PCF is only useful if it can trap light in the core due to the presence of band-gaps! The analysis thus performed is both much simpler than the methods associated with its multi-dimensional counterparts, most of which are numerical schemes which we will consider in Chapter 3.

This being said, the systems in this chapter are only simple examples of wider-reaching theory. Without much effort it is possible to consider some of the generalisations to these systems:

- Using a structure with edges parallel to the co-ordinate axes simplifies the analysis of the problem (particularly concerning determining the actions of the parametrised operators) however in doing so we also neglect the effect of the structure geometry. Introducing diagonal edges into a singular structure can lead to the opening of band-gaps in the fast-vertex scaling cases, and it is not hard to envisage graphs which not "centrally connected" or are even cyclic (like the honeycomb structure in Figure 1.1(b)). This is important for application to the design of optical fibres - fabrication techniques have greatly improved since the first optical fibres and so open up the possibility to explore more exotic geometric structure.

- The problem presented thus far has been a scalar-divergence equation, however an application to a physical system will require a formulation in terms of vector-valued functions on graphs. Whilst the idea of switching to a vector-valued function is not audacious, the effects this will have on the analysis of the systems may be more concerning. Vector-valued functions are almost always harder to work with than their scalar counterparts, and often result in the need to solve for the components in a coupled system of equations. There is also the need to investigate how to properly construct the singular-structure operator from the thin-structure operator we wish to approximate. This being said, with the additional complexity may come the possibility of unexplored effects which do not manifest in the scalar-case.

- A physical model for propagation also requires a time dependence, and hence a time derivative should appear in the operator. Whilst the effect of this is not fully understood, we can speculate on what it may mean for the singular-structure problem and previous analysis. The presence of a time-derivative immediately implies that the reduction to an ODE on the graph edges will no longer happen, as at the least the edge solutions will have to acknowledge the time-variation too. This will necessitate solution of a PDE on the edges, with the variables being the spatial

direction along the edge and time. Whilst such PDEs are not unapproachable, in general less is understood about the solution to PDEs than ODEs. Perhaps a more effective approach may be to trial an ansatz for the solution to the system, such as a Bloch-wave $e^{i(\mathbf{k}\cdot\mathbf{x}-\omega t)}$, which reduces the original system of equations to a set of coupled time-independent equations; although with this assumption again comes the potential to exclude certain effects that time-dependence may induce on the spectrum.

A combination of these considerations will need to be considered for a PCF model, as we will see in Chapter 4.

Chapter 3

Numerical Approach to the Thin-Structure Problem

Chapter 2 explored the application of the tools that can be used to analyse singular-structure problems, and obtain information about their spectra. The borderline case example will prove particularly useful here as it provides the effective problem for the thin-structure problem we will consider, in order to demonstrate the ability to estimate the spectrum of a 2-dimensional problem with that of a graph problem (as was claimed in Chapter 1). In this chapter we will explore the spectrum of a thin-structure problem on a periodic domain, in the finite-frequency approximation as the length scales $N \to \infty$, $\varepsilon \to 0$ such that $\varepsilon^\alpha N \to \gamma \in (0, \infty)$. This will involve an introduction to the Finite Element Method and a derivation of the finite-dimensional approximation to the eigenvalue problem, followed by some analysis of the resulting problem. Numerical results for the eigenfrequencies and eigenfunctions are presented for visualisation and to demonstrate that the spectra "fill-up" intervals in the positive real axis as $N \to \infty$, $\varepsilon \to 0$.

3.1 The Thin-Structure Problem

Suppose we have a periodic structure in $\mathbb{R}^2$, whose periodic unit cell is the unit square. The period cells themselves have microstructure of length scale ε and whose geometry composes a cross originating from the centre of the unit cell; whose arms are parallel to the co-ordinate axes, with width ε. Each arm of the cross meets the arc of a semi-circle of radius $\sqrt{\varepsilon}$; with the straight edge of each semicircle lying along the edge of the unit cell, and with the midpoint of the straight edge sharing the midpoint of the (respective) periodic cell edge. The unions of the cross and semicircles in each unit cell forms the domain. Note that the radius of the semicircles and widths of the arms of the cross are chosen so that we shall be in the borderline case of vertex- and edge-volume decay. This geometry is illustrated in Figure 3.1; and we denote these periodic unit cells by P_ε. Once again we seek to determine the spectrum of the operator $-\nabla^2 u$ on this domain, for $u \in H^1(\Omega)$, with zero-normal derivative boundary conditions imposed on the boundary.

Setting up the finite-frequency approximation (Section 1.3), let $N \in \mathbb{N}$, and consider the domain $\Omega_{\varepsilon,N} \subset [0, N]^2$ formed from stacking N^2 translated copies of P_ε into a square. We divide the boundary

$\partial\Omega_{\varepsilon,N}$ into two disjoint subsets:

$$\Gamma_{\mathrm{p}} := \partial\Omega_{\varepsilon,N} \cap (([0,N]) \cup ([0,N] \times \{0,N\})) \text{ and}$$
$$\Gamma_0 := \partial\Omega_{\varepsilon,N} \setminus \Gamma_{\mathrm{p}},$$

which are the interior boundary Γ_0 which outlines the holes in the domain; and the periodic boundary Γ_{p} which comprises the semicircle straight-edges which have periodic boundary conditions imposed on them. On $\Omega_{\varepsilon,N}$ we obtain the eigenvalue problem

$$-\nabla^2 u = \omega^2 u \quad \text{on } \Omega_{\varepsilon,N} \tag{3.1a}$$
$$\mathbf{n} \cdot \nabla u = 0 \quad \text{on } \Gamma_0 \tag{3.1b}$$
$$u \text{ is periodic across} \quad \Gamma_{\mathrm{p}}. \tag{3.1c}$$

3.2 Overview of the Finite Element Method

The geometry of the domain makes an analytic approach to the problem difficult, so we turn to numerical techniques to aid our analysis - in particular the Finite Element Method (FEM). The basis of the FEM is to write the boundary value problem (3.1) in the weak formulation, and then to solve the weak formulation on some finite-dimensional function space to obtain an approximate solution. The FEM has well-established theory, (in this report we follow [9]) and so we also provide statements of key convergence and error results.

We first define a mesh for our domain $\Omega_{\varepsilon,N}$, which is a set of triangles (called mesh-elements or simply elements) $\mathcal{T}$ whose vertices are called nodes (which form the set of nodes $\mathcal{N}$). The mesh must cover the entirely of $\bar{\Omega}_{\varepsilon,N}$, with the exception being the curved boundaries of the domain, which are approximated by a series of straight-lines (hence, the circular parts of the domain are approximated by n-gons). Additionally the intersection of two elements $\tau, \tau' \in \mathcal{T}$ must be either; the whole edge of two triangles, a single node $n \in \mathcal{N}$, or $\varnothing$. We define the diameter of the mesh as $h = \max_{\tau \in \mathcal{T}} h_\tau$ where h_τ is the diameter of the element τ (that is, the length of it's longest edge). Note that the periodicity of $\Omega_{\varepsilon,N}$ is encoded into the mesh, those elements τ which intersect Γ_{p} are identified with

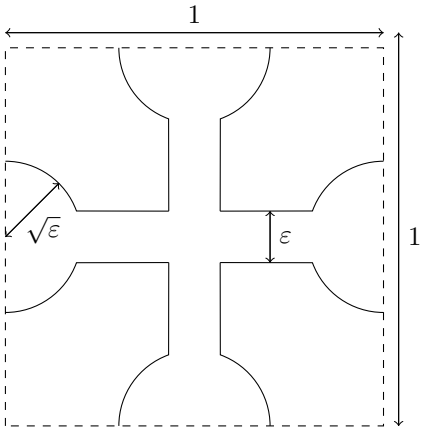

Figure 3.1: The unit cell of the periodic structure. The radius of the (semi-) circles is chosen so that the volume of the circles decays at the same rate as the volume of the tubes.

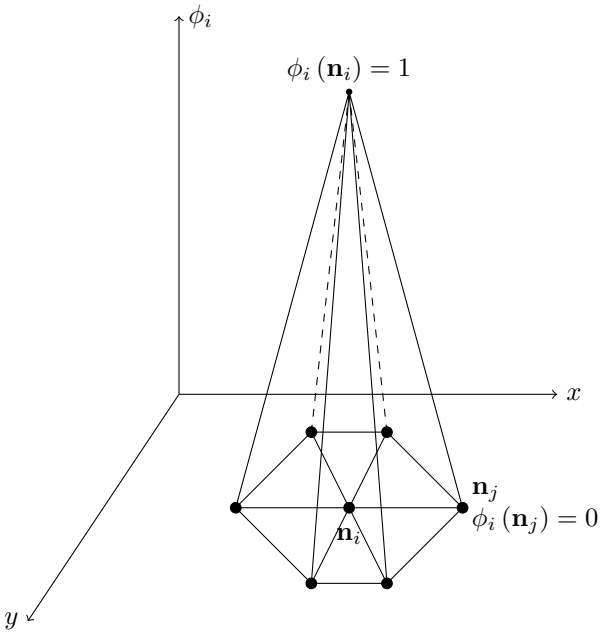

Figure 3.2: A typical choice for the basis functions ϕ_i is the 2-dimensional hat function. These functions are only non-zero on elements in $\mathcal{T}$ which have $\mathbf{n}_i$ as a vertex.

the elements τ' which intersect the corresponding periodic part of the boundary. Now define functions ϕ_i for each $\mathbf{n}_i \in \mathcal{N}$; by requiring that $\phi_i(\mathbf{n}_j) = \delta_{ij}$ and ϕ_i be linear[1][2] on each $\tau \in \mathcal{T}$. Typical ϕ_i are the 2-dimensional analogues of the "hat" functions, centred at each of the nodes - see the illustration in Figure 3.2. These functions serve as a basis for the (finite-dimensional) space

$$V_h = \left\{ v \in C\left(\bar{\Omega}_{\varepsilon,N}\right) \mid v\Big|_\tau \text{ is linear } \forall \tau \in \mathcal{T} \right\}.$$

For compactness we let $V = H^1(\Omega)$, and suppose we have a mesh $\mathcal{T}$ for $\Omega_{\varepsilon,N}$ with M nodes in a set $\mathcal{N}$ and mesh diameter h. Let $u \in V$ be a solution to the boundary value problem (3.1) and $v \in V$ an arbitrary element of V. To derive the weak formulation of (3.1a), we multiply through by v and integrate over $\Omega_{\varepsilon,N}$ to obtain

$$\int_{\Omega_{\varepsilon,N}} -v\nabla^2 u - \omega^2 uv \, \mathrm{d}x = 0 \quad \forall v \in V.$$

Applying the Divergence Theorem to the term involving the Laplacian gives

$$\int_{\Omega_{\varepsilon,N}} \nabla u \cdot \nabla v - \omega^2 uv \, \mathrm{d}x + \int_{\Gamma_0} v\left(\mathbf{n} \cdot \nabla u\right) \, \mathrm{d}S = 0 \quad \forall v \in V.$$

[1]In the sense that $\phi_i(\mathbf{x})$ is a linear combination of 1 and the components of $\mathbf{x}$.

[2]The FEM does not require linear interplants, and can be done with polynomial functions of any degree. We restrict to the case of linear interplants (degree 1 polynomials) for simplicity and computation cost.

Note here that only the integral over the non-periodic boundary appears, as the periodicity conditions are dealt with in the construction of the mesh. By (3.1b), $\mathbf{n} \cdot \nabla u = 0$ on Γ_0 and thus the surface integral is zero, and we arrive at

$$\int_\Omega \nabla u \cdot \nabla v - \omega^2 uv \, \mathrm{d}x = 0 \quad \forall v \in V \tag{3.2}$$

which is the aforementioned weak formulation of (3.1). We also introduce the canonical notation

$$a_1(u,v) = \int_{\Omega_{\varepsilon,N}} \nabla u \cdot \nabla v \, \mathrm{d}x$$
$$a_2(u,v) = -\omega^2 \int_{\Omega_{\varepsilon,N}} uv \, \mathrm{d}x,$$

which defines two[3] bilinear[4] forms $a_1, a_2 : V \times V \to \mathbb{R}$ whose sum comprises the left-hand-side of (3.2). The mesh $\mathcal{T}$ comes equipped with a space $V_h \subset V$ over which we solve the weak formulation numerically[5]. Denote the finite element approximation to u as u_h; and this approximate solution is the function $u_h \in V_h$ which solves

$$a_1(u_h, v_h) = a_2(u_h, v_h) \quad \forall v_h \in V_h. \tag{3.3}$$

As V_h is finite-dimensional and a_1, a_2 bilinear forms, it is sufficient to solve (3.3) for all $\phi_j, j \in \{1, ..., M\}$ rather than over all elements v_h of V_h. We may also write u_h as a sum of basis functions

$$u_h(x) = \sum_{\mathcal{I}} U_i \phi_i(x)$$

for constants U_i. Incorporating these insights into (3.3) it can be seen that finding the FEM approximation amounts to solving

$$\sum_{i=1}^{M} a_1(\phi_i, \phi_j) U_i = \omega^2 \sum_{i=1}^{M} a_2(\phi_i, \phi_j) U_i \quad \forall j \in \{1, ..., M\} \tag{3.4}$$

for the unknown constants U_i. (3.4) has a convenient matrix form $A^{(1)}\mathbf{U} = \omega^2 A^{(2)}\mathbf{U}$ where the matrices $A^{(k)}$ (the stiffness matrices) have entries

$$A^{(1)} = a_1(\phi_i, \phi_j) = \int_{\Omega_{\varepsilon,N}} \nabla\phi_i \cdot \nabla\phi_j \, \mathrm{d}x$$
$$A^{(2)} = a_2(\phi_i, \phi_j) = \int_{\Omega_{\varepsilon,N}} \phi_i \phi_j \, \mathrm{d}x$$

Hence we may find eigenfrequencies ω^2 and approximate eigenfunctions u_h by finding solutions to the (generalised) eigenvalue equation

$$A^{(1)}\mathbf{U} = \omega^2 A^{(2)}\mathbf{U}. \tag{3.5}$$

[3]Note that if we were not considering the eigenvalue problem, but rather had ω as a fixed parameter, it would be sufficient to only define a single bilinear form. However in order to solve the eigenvalue problem, IE for unknown ω and u, we are required to separate terms involving ω from terms that do not.

[4]The linearity properties are easily proved directly from the definitions of a_1 and a_2.

[5]Note that linear interplants have trivial second derivative, and so are elements of $H^2(\Omega_{\varepsilon,N})$ too.

Typically this is done using an iterative method, as direct solution is computationally expensive and unstable. It is for this reason that we leave the problem in a form that does not involving matrix inverses (even though it will be shown that these exist as $A^{(1)}, A^{(2)}$ are symmetric positive definite) which are computationally expensive, and become unstable when a matrix has a significant concentration of eigenvalues in an interval.

When performing these numerics the domain was setup so that $\varepsilon = \frac{1}{10N}$; ensuring that $\varepsilon N \to \frac{1}{10} \in (0\infty)$, that the thin-structure setup was realisable without overlaps from different components, and placing us in a regime which has the problem from Section 2.2 as its effective problem. The FEM was implemented in Python 3.6 using software from FEniCS [10] to construct the stiffness matrices. The eigenvalues in (3.5) were found using SciPy's eigenvalue solvers [11].

3.3 Analysis

The choice of basis functions ϕ_i results in the stiffness matrices being sparse. In particular, the products $\phi_i\phi_j$ and $\nabla\phi_i \cdot \nabla\phi_j$ are only non-zero when the nodes $\mathbf{n}_i$ and $\mathbf{n}_j$ are shared by an element[6]. This allows us to re-write the integrals over the whole domain $\Omega_{\varepsilon,N}$ as a sum of integrals over those elements $\tau \in \mathcal{T}$ such that $\mathbf{n}_i, \mathbf{n}_j$ are vertices of τ, and hence provides this sparsity. This is particularly useful when solving (3.5) numerically, as it allows for efficient matrix storage. However the approximation of the infinite-dimensional space $H^1(\Omega)$ by V_h means that the FEM can never be used to obtain the entire (analytic) spectrum of the original operator. As the matrices $A^{(1)}, A^{(2)}$ are $M \times M$, the number of nodes places an upper limit on the number of eigenvalues we can find. Refinements to the mesh (hence placement of additional nodes) allow deeper exploration of the spectrum, however this must be counterbalanced with the computational effort of finding the complete set of solutions to (3.5).

A well established bound for the error in the FEM is given in the Aubin-Nitsche theorem (see for example [9] for formal setup and proof). For a mesh $\mathcal{T}$ with diameter h, the error of the approximate solution u_h in the $L^2(\Omega_{\varepsilon,N})$-norm is bounded by

$$||u - u_h||_{L^2(\Omega_{\varepsilon,N})} \leq Ch^2 ||u||_{H^2(\Omega_{\varepsilon,N})}$$

provided that the mesh has some regularity[7]. In practice this bound is not particularly useful for choosing a mesh so that it produces an approximation correct to a certain error, as it requires knowledge of the solution u and it's $H^2(\Omega_{\varepsilon,N})$ norm. However it does establish that a finer mesh (smaller h) reduces the error in the approximation, and the convergence to the solution u (in the $L^2(\Omega_{\varepsilon,N})$-norm) is is quadratic.

Trivially noting that the bilinear forms a_1 and a_2 are symmetric in their arguments, we have that $A^{(1)}$ and $A^{(2)}$ are symmetric. Pursuing justification that the equation (3.5) has solutions, we prove positive definiteness of the stiffness matrix $A^{(1)}$. First we prove that the bilinear forms a_1 is V-elliptic, that is that there exists a constant $c > 0$ such that

$$a_1(v, v) \geq c_1 ||v||_V .$$

[6]This is taken to include the case $i = j$.

[7]Precisely, the mesh $\mathcal{T}$ must be shape-regular: there exists a constant $C > 0$ such that $\frac{h_\tau^2}{\mu(\tau)} < C$ for all $\tau \in \mathcal{T}$, where $\mu(\tau)$ denotes the area of the element τ. Intuitively, this ensures that the elements cannot become arbitrarily long and thin.

This is done by an application of the Poincaré inequality, $||v||^2_{L^2(\Omega_{\varepsilon,N})} \leq C\,||\nabla v||^2_{L^2(\Omega_{\varepsilon,N})}$ and recognising that $a_1(v,v) = ||\nabla v||^2_{L^2(\Omega_{\varepsilon,N})}$:

$$\begin{aligned} ||v||^2_V &= ||\nabla v||^2_{L^2(\Omega_{\varepsilon,N})} + ||\nabla v||^2_{L^2(\Omega_{\varepsilon,N})} \\ &\leq (C+1)\,||\nabla v||^2_{L^2(\Omega_{\varepsilon,N})} \\ \Leftrightarrow \frac{1}{C+1}\,||v||^2_V &\leq ||\nabla v||^2_{L^2(\Omega_{\varepsilon,N})} = a_1(v,v)\,. \end{aligned}$$

$\frac{1}{C+1} > 0$ as $C > 0$, and as $v \in V$ was arbitrary, a_1 is V-elliptic. Now for any vector $\mathbf{v} = (v_1, ..., v_M)^\top \neq \mathbf{0}$, we have that

$$\begin{aligned} \mathbf{v}^\top A^{(1)}\mathbf{v} &= \sum_{i=1}^M \sum_{j=1}^M v_i v_j a_1(\phi_i, \phi_j) \\ &= a_1\left(\sum_{i=1}^M v_i\phi_i, \sum_{j=1}^M v_j\phi_j\right) \qquad \text{(by bilinearity)} \\ &= a_1(v_h, v_h) \geq ||v_h||_V > 0 \end{aligned}$$

where $v_h \in V_h \subset V$ is the element of V_h with basis representation $v_h = \sum_{i=1}^M v_i\phi_i$. Thus $A^{(1)}$ is positive definite. Positive-definiteness of $A^{(2)}$ is more easily established, as for any $\mathbf{v} = (v_1, ..., v_M)^\top \neq \mathbf{0}$ and setting $v_h = \sum_{i=1}^M v_i\phi_i$ we have

$$\begin{aligned} \mathbf{v}^\top A^{(2)}\mathbf{v} &= \sum_{i=1}^M \sum_{j=1}^M v_i v_j a_2(\phi_i, \phi_j) \\ &= a_2\left(\sum_{i=1}^M v_i\phi_i, \sum_{j=1}^M v_j\phi_j\right) = a_2(v_h, v_h) \\ &= \int_{\Omega_{\varepsilon,N}} v_h^2 \,\mathrm{d}x \\ &> 0; \end{aligned}$$

where the final inequality is strict because if $\mathbf{v} \neq \mathbf{0}$ the function v_h cannot be the zero function as the ϕ_i form a basis of V_h, and hence the continuous and non-identically zero function $v_h^2 \geq 0$ cannot have zero integral over $\Omega_{\varepsilon,N}$. This give us positive-definiteness of $A^{(2)}$ as well. Now as $A^{(1)}$ is symmetric positive definite, so it is invertible with symmetric positive-definite inverse $\left(A^{(1)}\right)^{-1}$. Hence solving (3.5) is equivalent to solving the eigenvalue equation

$$B\mathbf{U} = \omega^2\mathbf{U} \tag{3.6}$$

where the matrix $B = \left(A^{(1)}\right)^{-1} A^{(2)}$ is the product of two symmetric positive-definite matrices. Thus B has positive eigenvalues[8].

[8] A short proof of this statement is as follows: Let A_1, A_2 be symmetric positive-definite matrices. Then A_2 has symmetric positive-definite matrix square root $A_2^{\frac{1}{2}}$. Hence we can express the product $A_1A_2 = A_2^{-\frac{1}{2}}\left(A_2^{\frac{1}{2}}A_1A_2^{\frac{1}{2}}\right)A_2^{\frac{1}{2}}$, so A_1A_2 is similar to the symmetric positive-definite matrix $A_2^{\frac{1}{2}}A_1A_2^{\frac{1}{2}}$, hence has the same eigenvalues. The eigenvalues of a symmetric positive-definite matrix are strictly positive, hence so are the eigenvalues of A_1A_2.

To conclude we present some numerical results for the spectra and associated eigenfunctions. In order to demonstrate that the spectrum is becoming increasingly dense along the positive real line, we produce an integrated spectral density plot Figure 3.3 for the region $(0, 2\pi)$. The integrated spectral density plot shows many eigenvalues lie below each value along the positive real line, normalised to the volume (in this case area) of $\Omega_{\varepsilon,N}$. This plot provides us with information on how quickly the spectrum is "filling-up" the positive real line as N increases - at the least the plots demonstrate that this *is* happening. This is to be expected given the analysis of Section 2.2; which is the effective problem for the thin-structure problem we consider here, and so we expect the spectrum to converge to (something close to) the band-gap spectrum obtained in that section. We can see some evidence of this in Figure 3.3; the integrated density remains constant over the interval $\omega \in (\pi, 1.25\pi)$ which is consistent with the aforementioned analysis of the band-gap spectrum (each band terminating at $n\pi$). If an analytic expression for the integrated density of states available, we could obtain the corresponding density of states for each spectrum which shows how the eigenvalues cluster about various points on the positive real line. Unfortunately these plots are estimated from the numerical results to (3.5), so instead we must turn to histograms to estimate the distribution along the positive real line of the eigenvalues. Some examples of these are shown in Figure 3.4 (these are in terms of the eigenfrequencies, which have been divided by π to aid in visualising the spectrum). In these examples the smallest 1000 eigenfrequencies were computed for each domain, and one can again notice that as N increases the spectrum becomes increasingly dense. The choice to only compute 1000 eigenfrequencies was due to the available computer resources at the time; the system for $N = 2, 5, 10$ had $4005, 58096, 446022$ nodes and $8046, 104244, 893621$ elements respectively, and so determining the full spectra was unfeasible[9]. Also plotted are some of the FEM solutions for the $N = 2$ eigenfunctions (Figure 3.5), for visualisation. Computationally there is no further difficulty in obtaining the eigenfunctions having obtained the eigenvalues as they are computed in the same algorithm, however higher values of N result in it being difficult to see the variation of the eigenfunctions along the "tubes".

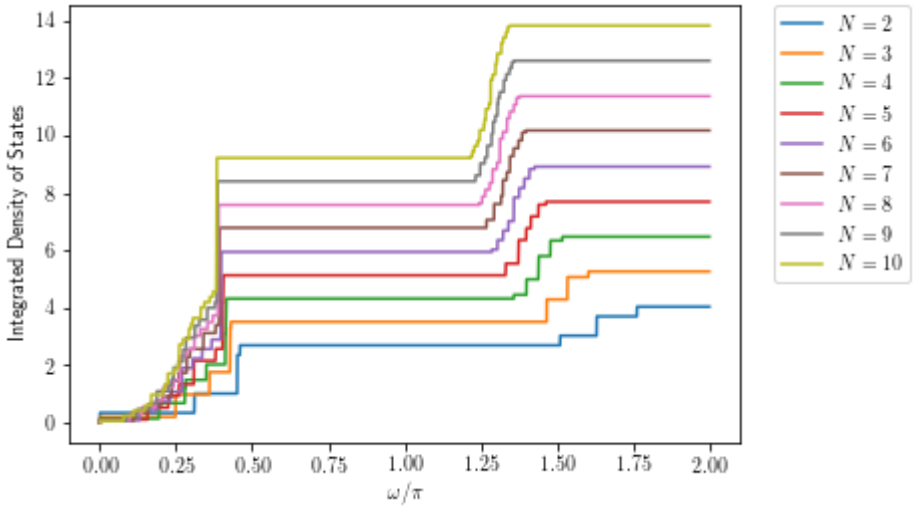

Figure 3.3: Integrated spectral density plot for various domains. The increasing density of the spectrum can be seen from visual inspection.

[9]To work around this problem and take the analysis further, one may chose to examine the structure of the stiffness matrices to determine whether faster algorithms can be used.

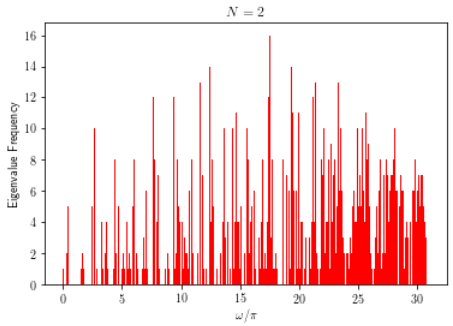

(a) Smallest 1000 eigenfrequencies for the $N = 2$ domain.

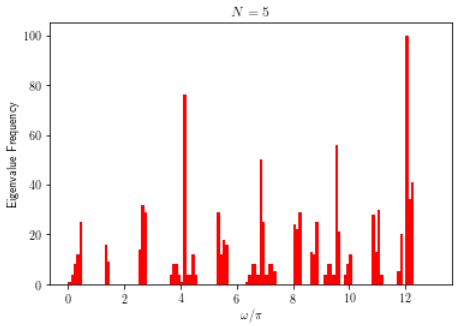

(b) Smallest 1000 eigenfrequencies for the $N = 5$ domain.

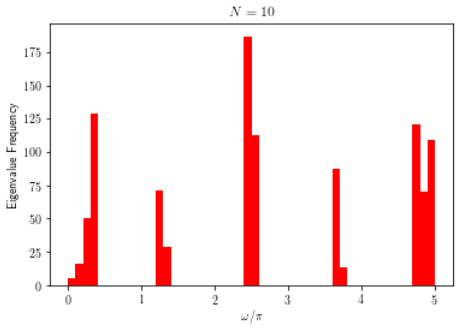

(c) Smallest 1000 eigenfrequencies for the $N = 10$ domain.

Figure 3.4: The smallest 1000 eigenfrequencies for various domains. Note that as N increases the spectrum becomes increasingly dense; the 1000^{th} eigenfrequency in the $N = 10$ problem is approximately 6 times smaller than it's $N = 2$ counterpart.

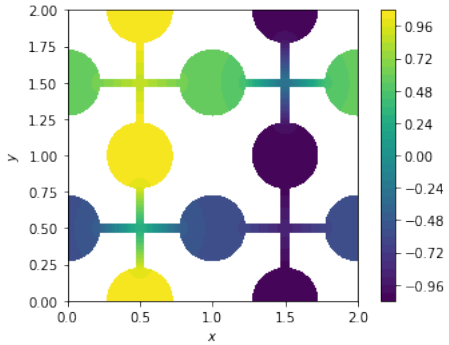

(a) The eigenfunction for the eigenfrequency $\omega = 0.9736174525997192$ in the $N = 2$ domain (3^{rd} smallest eigenfrequency).

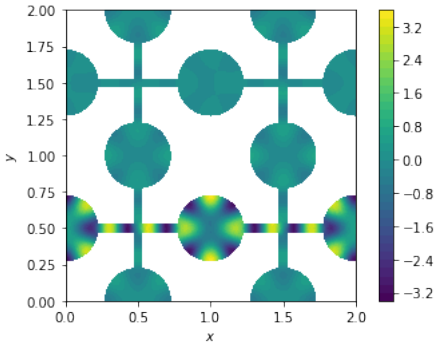

(b) The eigenfunction for the eigenfrequency $\omega = 25.37447775539648$ in the $N = 2$ domain (125^{th} smallest eigenfrequency).

Figure 3.5: Visualisation of the eigenfunctions corresponding to the 3^{rd} and 125^{th} eigenfrequencies, in the $N = 2$ domain. Note that the higher-ω eigenfunction varies more rapidly in the non-zero areas than it's counterpart.

Chapter 4

Conclusion and Direction of Further Work

4.1 Synthesis of Ideas and Discussion

As indicated in Chapter 1, a hollow-core PCF can be thought of as a periodic, thin-structure material occupying a fixed domain. We can represent this mathematically using a domain Ω with holes, which we interpret as inclusions (of the solid-core material) or as vacuum (hollow-core) - for simplicity we will discuss the hollow-core case. Then we are interested in determining which frequencies of light will be trapped by the fibre, due to the choice of PCF material and geometry of Ω. We will use the system of Maxwell equations,

$$\nabla \wedge \mathbf{E} = \frac{\partial}{\partial t}\left(\mu \mathbf{H}\right), \quad \nabla \wedge \mathbf{H} = -\frac{\partial}{\partial t}\left(\varepsilon_{\mathrm{p}} \mathbf{E}\right), \tag{4.1}$$

as the basis for this model; as before (Section 1.1) denotes the electric $\mathbf{E}$ and magnetic $\mathbf{H}$ fields, ε_{p} and μ the electric permittivity and magnetic permeability of the medium the light is propagating in. This problem can be formulated in the homogenisation setting (Section 1.3) by identifying a suitable period cell and introducing appropriate length scales ε and N. From Section 1.4 we know that we can gain knowledge about the spectrum of a thin-structure problem from analysis of a related singular-structure problem (provided the appropriate vertex and edge scaling is accounted for), which is more often open to an analytic approach. Therefore the design of the PCF (hence the domain Ω) admits some analysis of its spectrum, and so gain knowledge of the frequencies of light which the PCF is expected to trap. Schematically this is illustrated in Figure 4.1, and in what follows we will discuss extending the content of this report to the setting just described. Note that since we are working with a finite domain with a large number of periods, it will be more appropriate to work in the high-frequency approximation during the following discussion. Furthermore, in this section we assume we have a PCF design in the form of a periodic domain Ω and the corresponding periodic graph $\mathbb{G}$ (that arises from finding the corresponding singular structure). We let Ω_N and $\mathbb{G}_N$ denote the high-frequency approximation domains for each $N \in \mathbb{N}$ (that is, the finite domain filled with N copies of the unit cell stacked in each direction), see Section 1.3.

A simple formulation begins using the standard assumption in fibre-optics that the fibre is effectively a 2 dimensional periodic-structure in the (x, y) plane, extended as a prism into the third (z) dimension. Analysis of the 2D structure will result in the study of 2-dimensional periodic structures, much like the example studied in Chapter 2 and Chapter 3, and hence will admit an analysis along

similar lines to these examples. Within this there is scope to investigate and quantify the effect that the geometry of the microstructure has any the resulting spectrum. There is also the need to consider the additional complexities that a model based on (4.1) introduces, which have been touched on in Section 2.3. Foremost is that the Maxwell system is a vector-valued, time-dependant system unlike the elliptic scalar-divergence operators that we have considered thus far. One may take a similar line of analysis to [3] and consider an analysis of Bloch waves of the form

$$\mathbf{E} = E(x,y)\, e^{i(k_p z - \omega t)},$$
$$\mathbf{H} = H(x,y)\, e^{i(k_p z - \omega t)}.$$

Upon substituting this ansatz into (4.1) we are left with a set of coupled time-independent PDEs for the amplitude coefficients $E = (E_1, E_2, E_3)^\top$, $H = (H_1, H_2, H_3)^\top$:

$$\begin{aligned}
i\omega\varepsilon_{\mathrm{p}} E_1 &= \frac{\partial}{\partial y} H_3 - ik_p H_2, & -i\omega\mu H_1 &= \frac{\partial}{\partial y} E_3 - ik_p E_2,\\
i\omega\varepsilon_{\mathrm{p}} E_2 &= -\frac{\partial}{\partial x} H_3 + ik_p H_1, & -i\omega\mu H_2 &= -\frac{\partial}{\partial x} E_3 + ik_p E_1,\\
i\omega\varepsilon_{\mathrm{p}} E_3 &= \frac{\partial}{\partial x} H_2 - \frac{\partial}{\partial y} H_1, & -i\omega\mu H_3 &= \frac{\partial}{\partial x} E_2 - \frac{\partial}{\partial y} E_1,
\end{aligned}$$

and which can then be formulated on the corresponding singular structure and analysis akin to that in Chapter 2 can be performed. It should be noted that the system presented above admits further

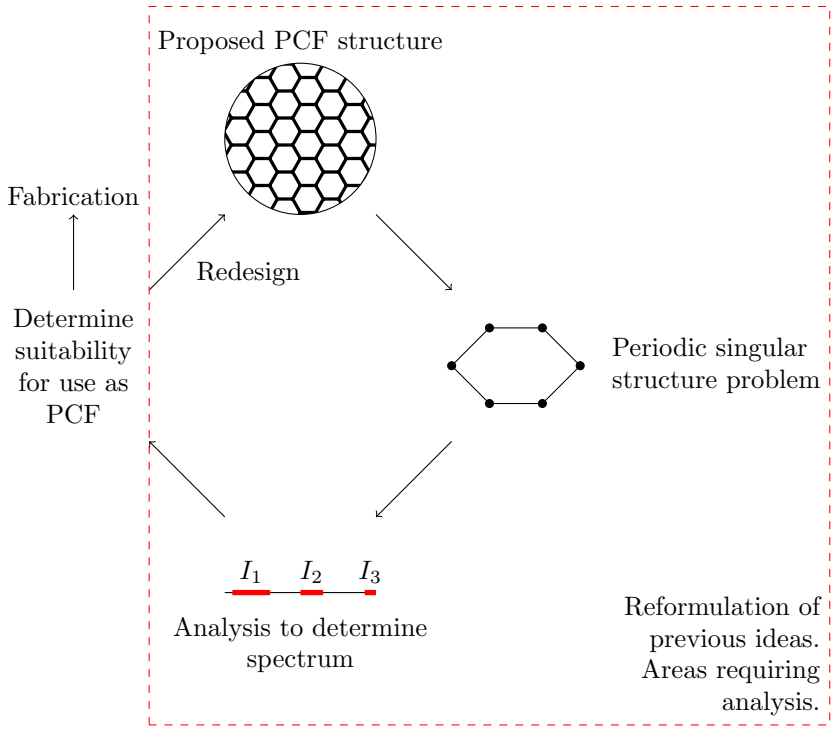

Figure 4.1: A diagram to illustrate how the concepts and theory presented in the preceeding chapters can be turned into a model of PCFs. The dashed-red box contains the areas which future work will focus on.

manipulation into a system involving only E_3, H_3 and their partial derivatives, which may also be exploited. There are several other lines of investigation at this point:

1. The Maxwell system also presents a system of coupled PDEs rather than the single PDE that has been considered thus far. In principle dealing with this complication is straightforward, as it is not hard to imagine generalising the process in Chapter 2 to systems of equations on the edges of the graph. In practice it may complicate the analysis that can be done, particularly if the resulting systems involve a large number of unknown coefficients or result in equations that do not have closed-form solutions[1].

2. Alternatively we may leave the time-dependence in the system and look to infer the resulting operator on the edges of the singular structure. Determining the operator which describes the differential operator on the singular-structure edges and vertex boundary conditions will require formal asymptotic expansion and analysis on the corresponding thin-structure problem.

Hence the focus of this first formulation should be to derive the appropriate singular-structure problem from the thin-structure problem it aims to approximate, derive the appropriate convergence results which justify its used, and then seek to determine (analytically or numerically), whether a quantifiable relation between the geometry of the structure and the characteristics of the spectrum exists.

Speculating beyond the 2-dimensional model, there is also the possibility of breaking with the assumption that the fibre is extended exactly parallel to the z-direction. In these cases, one may introduce an z-axial "twist" to the fibre microstructure; so the (x, y)-plane structure is rotating through an angle θ per unit length in the z-axis (Figure 4.2). This system is again governed by Maxwell's equations, and again has a 2-dimensional periodic structure as its cross section. However the twist will produce an effect on the spectrum and hence the frequencies the fibre can trap light at. Physically this may represent the effect of faults in the fabrication process; but also generalises the above discussion of the effect of fibre geometry on the spectrum to three dimensions. If treating this model in the former context (fabrication faults), one may elect to analyse the effect of θ being small and random, and look to quantify the resulting effects on the spectrum. The effect could be modelled approximately by sampling θ and running numerical solvers (a Monté Carlo approach), or alternatively from an analytical perspective involving interplay between probability theory and extensions to the theory in Chapter 1. If instead treating the model in the latter case; one would be looking to achieve much the same outcomes as the original 2-dimensional model, a sense of how the geometry can be effectively chosen to provide a PCF with the desired spectrum. Additionally one of the key features of optical fibres is that they can direct light around corners; and in order for PCFs to compete with optical fibres they need to offer this feature as well. This offers another 3-dimensional system to consider; in this the fibre is not parallel to the z-axis but instead curves through some angle. The primary concern in these problems will be to measure the optical loss along the fibre, and (particularly in the twisted fibre case) whether the geometry down the fibre has a decided effect on the spectrum, hence the operating frequencies. To approach these problems, one may first chose to employ numerical techniques as in Chapter 3 — the finite element method is perfectly applicable in 3-dimensions and deals with complex domain geometry. However this does not provide us with an analytical model that can be used to explain any of the features we may observe. For this we may turn to the previous analysis on the singular-structure problem for the (x, y)-geometry, a simple model could envisage the geometry along the fibre as a (curved) rectangular "sheet", where the profile of the solution along the x, y plane is known — coming from the edge solution on the graph. Clearly this runs into complications when the fibre has a twist, as we would need to deal with the rotation along the fibre with an appropriate set of co-ordinates. However such models have the potential to provide

[1] As was the case in Section 2.2, determining the spectrum itself had to be done numerically.

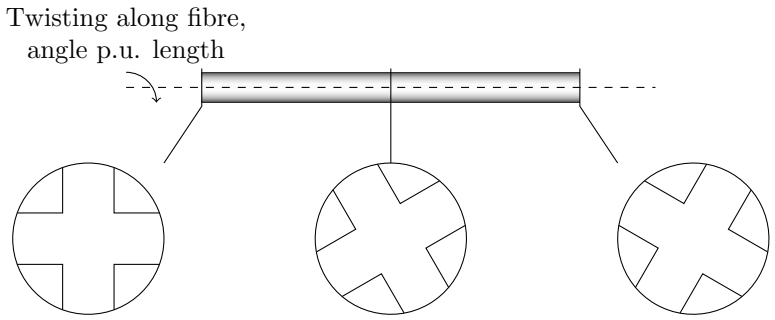

Figure 4.2: Illustration of the extension into 3 dimensions, assuming a twist in the fibre. The (x, y)-plane's structure is rotated through some angle per unit length, represented schematically by the unit cells shown below the fibre.

highly informative models for the loss in PCFs, and whether they can match the desirable features of optical fibres (such as that of guiding light around corners).

4.2 Closing Remarks

This report has demonstrated some of the key concepts and methods that provide potential for a new model of PCFs which can be used to inform their design. These models incorporate theory from quantum graphs and homogenisation theory present to obtain information about complex thin-structure problems from comparatively more accessible singular-structure problems. In turn the information that can be gained from this model can feedback into the design process for PCFs, and also look to identify the cause-effect relationship of fibre-geometry to spectrum. Formulations in both a 2-dimensional and 3-dimensional setting have been given and briefly discussed with the aim of motivating future study in these directions. What is clear is that this presents an exciting method for PCFs, and reasons for extending the existing mathematical theory it is associated with.

Bibliography

[1] Jonathan C Knight. Photonic Crystal Fibres. *Nature*, 424(6950):847, 2003.

[2] Philip Russell. Photonic Crystal Fibers. *Science*, 299(5605):358–362, 2003.

[3] S. Cooper, I. Kamotski, and V. Smyshlyaev. On band gaps in photonic crystal fibers. *ArXiv e-prints*, November 2014.

[4] Sofiane Soussi. Modeling photonic crystal fibers. *Advances in Applied Mathematics*, 36(3):288–317, 2006.

[5] Gregory Berkolaiko and Peter Kuchment. *Introduction to quantum graphs*. Number 186. American Mathematical Soc., 2013.

[6] Yulia Ershova. Homogenisation for Graphs Peroidic in One Dimension. Pre-print of work conducted at the University of Bath, 2018.

[7] Pavel Exner and Olaf Post. Convergence of spectra of graph-like thin manifolds. *Journal of Geometry and Physics*, 54(1):77–115, 2005.

[8] Peter Kuchment and Hongbiao Zeng. Convergence of spectra of mesoscopic systems collapsing onto a graph. *Journal of Mathematical Analysis and Applications*, 258(2):671–700, 2001.

[9] Claes Johnson. *Numerical solution of partial differential equations by the finite element method*. Courier Corporation, 2012.

[10] Martin S. Alnæs, Jan Blechta, Johan Hake, August Johansson, Benjamin Kehlet, Anders Logg, Chris Richardson, Johannes Ring, Marie E. Rognes, and Garth N. Wells. The fenics project version 1.5. *Archive of Numerical Software*, 3(100), 2015.

[11] Eric Jones, Travis Oliphant, Pearu Peterson, et al. SciPy: Open source scientific tools for Python, 2001–. Online.